LYAPUNOV-BASED CONTROL OF A ROBOT AND MASS-SPRING SYSTEM UNDERGOING AN IMPACT COLLISION

By

CHIEN-HAO LIANG

A THESIS PRESENTED TO THE GRADUATE SCHOOL
OF THE UNIVERSITY OF FLORIDA IN PARTIAL FULFILLMENT
OF THE REQUIREMENTS FOR THE DEGREE OF
MASTER OF SCIENCE

UNIVERSITY OF FLORIDA

2007

To my wife Yen-Chen and son Hsu-Chen who constantly filled me with love and joy.

ACKNOWLEDGMENTS

I would like to express my gratitude to my advisor, mentor, and friend, Dr. Warren E. Dixon for introducing me with the interesting field of Lyapunov-based control. As an advisor, he provided the necessary guidance and allowed me to try some stupid ideas during my research. As a mentor, he helped me understand the high pressure of working in a professional environment and was willing to give me time to learn and adjust. I feel fortunate in getting the opportunity to work with him.

I also appreciate my committee members Dr. Carl D. Crane III and Dr. Gloria J. Wiens for the time and help they provided.

I would like to thank all my friends for their support and encouragement. I especially thank my friend Guoqiang Hu for being my listener and mentor both in the research and daily life for the last two years. I would also like to thank my colleague Keith Stegath for helping me out on those difficult days when I was doing my experiments. Without him, I cannot accomplish these experiments. I would like to thank my colleague Darren Aiken for his caring during my first year in U.S. I express my gratitude to Keith Dupree for helping me out on my research. I also express my gratitude to Parag Patre and Will Mackunis who filled my daily life with joy.

Finally I would like to thank my parents for their unconditional love and support, my wife Yen-Chen for the support and joy she always brought to me, and my son Hsu-Chen for his hug, kiss, and smile. Their love, understanding, patience and personal sacrifice made this thesis possible.

TABLE OF CONTENTS

page

ACKNOWLEDGMENTS iv

LIST OF FIGURES vii

CHAPTER

ABSTRACT ix

1 INTRODUCTION 1

1.1 Introduction 1
1.2 Dynamic Model 7

2 LYAPUNOV-BASED CONTROL OF A ROBOT AND MASS-SPRING SYSTEM UNDERGOING AN IMPACT COLLISION 11

2.1 Error System and Control Development 11
2.1.1 Control Objective 11
2.1.2 Closed-Loop Error System 12
2.2 Stability Analysis 14
2.3 Experimental Results 19
2.4 Concluding Remarks 25

3 GLOBAL ADAPTIVE LYAPUNOV-BASED CONTROL OF A ROBOT AND MASS-SPRING SYSTEM UNDERGOING AN IMPACT COLLISION 26

3.1 Properties and Assumptions 27
3.2 Error System and Control Development 28
3.2.1 Control Objective 28
3.2.2 Closed-Loop Error System 29
3.3 Stability Analysis 33
3.4 Experimental Results 39
3.5 Concluding Remarks 46

4 AN IMPACT FORCE LIMITING ADAPTIVE CONTROLLER FOR A ROBOTIC SYSTEM UNDERGOING A NON-CONTACT TO CONTACT TRANSITION 47

4.1 Properties 48
4.2 Error System and Control Development 48

4.2.1 Control Objective 49
4.2.2 Closed-Loop Error System 50
4.3 Stability Analysis 51
4.4 Experimental Results 57
4.5 Concluding Remarks 63

5 CONCLUSION AND RECOMMENDATIONS 64

APPENDIX

A THE EXPRESSION OF $\ddot{x}_{rd1}$ IN SECTION 2.1 66

B THE EXPRESSION OF $\ddot{x}_{rd1}$ IN SECTION 3.2 68

REFERENCES 69

BIOGRAPHICAL SKETCH 74

LIST OF FIGURES

Figure page

1–1 The Mass-Spring Robot (MSR) system is an academic example of an impact between two dynamic systems. 8

2–1 Top view of experimental testbed including: (1) mass-spring, (2) LVDT, (3) capacitance probe, (4) link 1, (5) motor 1, (6) link 2, (7) stiff spring mechanism, (8) mass. 20

2–2 Side view of experimental testbed 20

2–3 The spring-mass and robot errors $e(t)$. Plot (a) indicates the position error of the robot tip along the X_1-axis (i.e., $e_{r1}(t)$), (b) indicates the position error of the robot tip along the X_2-axis (i.e., $e_{r2}(t)$), and (c) indicates the position error of the spring-mass (i.e., $e_m(t)$). 23

2–4 Computed control torques $J^T(q)F(t)$ for the (a) base motor and (b) second link motor. 23

2–5 Applied control torques $J^T(q)F(t)$ (solid line) versus computed control torques (dashed line) for the (a) base motor and (b) second link motor. . 24

2–6 Computed desired robot trajectory, $x_{rd1}(t)$. 24

2–7 Contact ($\Lambda = 1$) and non-contact ($\Lambda = 0$) conditions for the robot and mass-spring system. 25

3–1 The mass-spring and robot errors $e(t)$. Plot (a) indicates the position error of the robot tip along the X_1-axis (i.e., $e_{r1}(t)$), (b) indicates the position error of the robot tip along the X_2-axis (i.e., $e_{r2}(t)$), and (c) indicates the position error of the mass-spring (i.e., $e_m(t)$). 41

3–2 The mass-spring and robot errors $e(t)$ during the initial two seconds. . . 42

3–3 Computed control torques $J^T(q)F(t)$ for the (a) base motor and (b) second link motor. 42

3–4 Applied control torques $J^T(q)F(t)$ (solid line) versus computed control torques (dashed line) for the (a) base motor and (b) second link motor. . 43

3–5 Computed desired robot trajectory, $x_{rd1}(t)$. 43

3–6 Unitless parameter estimate $\hat{\theta}_{dk}(t)$ introduced in (3–13). 44

3–7 Estimate for the unknown constant parameter vector $\hat{\theta}_r(t)$. (a) $\hat{\theta}_{r10}(t) = K_I$, (b) $\hat{\theta}_{r4}(t) = \frac{K_I m_s}{m}$, (c) $\hat{\theta}_{r1}(t) = \frac{K_I m_1}{m}$, and (d) $\hat{\theta}_{r7}(t) = \frac{K_I m_2}{m}$, where m_1, $m_2 \in \mathbb{R}$ denote the mass of the first and second link of the robot, $m_s \in \mathbb{R}$ denotes the mass of the motor connected to the second link of the robot, and $m \in \mathbb{R}$ denotes the mass of the mass-spring system. . . . 44

3–8 Estimate for the unknown constant parameter vector $\hat{\theta}_r(t)$. (a) $\hat{\theta}_{r5}(t) = \frac{k_s m_s}{m}$, (b) $\hat{\theta}_{r2}(t) = \frac{k_s m_1}{m}$, and (c) $\hat{\theta}_{r8}(t) = \frac{k_s m_2}{m}$. 45

3–9 Estimate for the unknown constant parameter vector $\hat{\theta}_r(t)$. (a) $\hat{\theta}_{r6}(t) = m_s$, (b) $\hat{\theta}_{r3}(t) = m_1$, and (c) $\hat{\theta}_{r9}(t) = m_2$. 45

4–1 The mass-spring and robot errors $e(t)$. Plot (a) indicates the position error of the robot tip along the X_1-axis (i.e., $e_{r1}(t)$), (b) indicates the position error of the robot tip along the X_2-axis (i.e., $e_{r2}(t)$), and (c) indicates the position error of the mass-spring (i.e., $e_m(t)$). 59

4–2 Applied control torques $J^T(q)F(t)$ for the (a) base motor and (b) second link motor. 59

4–3 Applied control torques $J^T(q)F(t)$ for the (a) base motor and (b) second link motor during the first 0.8 second. 60

4–4 Computed desired robot trajectory, $x_{rd1}(t)$. 60

4–5 Parameter estimate $\hat{\theta}_{dk}(t)$ introduced in (3–13). 61

4–6 Estimate for the unknown constant parameter vector $\hat{\theta}_r(t)$. (a) $\hat{\theta}_{r10}(t) = K_I$, (b) $\hat{\theta}_{r4}(t) = \frac{K_I m_s}{m}$, (c) $\hat{\theta}_{r1}(t) = \frac{K_I m_1}{m}$, and (d) $\hat{\theta}_{r7}(t) = \frac{K_I m_2}{m}$, where m_1, $m_2 \in \mathbb{R}$ denote the mass of the first and second link of the robot, $m_s \in \mathbb{R}$ denotes the mass of the motor connected to the second link of the robot, and $m \in \mathbb{R}$ denotes the mass of the mass-spring system. . . . 61

4–7 Estimate for the unknown constant parameter vector $\hat{\theta}_r(t)$. (a) $\hat{\theta}_{r5}(t) = \frac{k_s m_s}{m}$, (b) $\hat{\theta}_{r2}(t) = \frac{k_s m_1}{m}$, and (c) $\hat{\theta}_{r8}(t) = \frac{k_s m_2}{m}$. 62

4–8 Estimate for the unknown constant parameter vector $\hat{\theta}_r(t)$. (a) $\hat{\theta}_{r6}(t) = m_s$, (b) $\hat{\theta}_{r3}(t) = m_1$, and (c) $\hat{\theta}_{r9}(t) = m_2$. 62

Abstract of Thesis Presented to the Graduate School
of the University of Florida in Partial Fulfillment of the
Requirements for the Degree of Master of Science

LYAPUNOV-BASED CONTROL OF A ROBOT AND MASS-SPRING SYSTEM UNDERGOING AN IMPACT COLLISION

By

Chien-Hao Liang

May 2007

Chair: Warren E. Dixon
Major Department: Mechanical and Aerospace Engineering

The problem of controlling a robot during a non-contact to contact transition has been a historically challenging problem that is practically motivated by applications that require a robotic system to interact with the environment. If the contact dynamics are not properly modeled and controlled, the contact forces could result in poor system performance and instabilities. One difficulty in controlling systems subject to non-contact to contact transition is that the dynamics are different when the system status changes suddenly from the non-contact state to a contact state. Another difficulty is measuring the contact force, which can depend on the geometry of the robot, the geometry of the environment, and the type of contact. The appeal of systems with contact conditions is that short-duration effects such as high stresses, rapid dissipation of energy, and fast acceleration and deceleration may be achieved from low-energy sources.

Over the last two decades, many researchers have investigated the modeling and control of contact systems. Two trends are apparent after a comprehensive survey of contact systems in control literature. Most controllers target contacts with a static environment for a fully actuated system. Many researchers also

exploit switching or discontinuous controllers to accommodate for the contact conditions. Motivation exists to explore alternative control strategies because impacts between the robot and the static environment cannot represent all the impact system applications such as the capture of disabled satellites, spaceport docking, manipulation of non-rigid bodies, and so on, and discontinuous controllers require infinite control frequency (i.e., exhibit chattering) or yield degraded stability results (i.e., uniformly ultimately bounded). As stated previously, it is necessary to consider the impact control between two dynamic systems.

This research considers a class of fully actuated dynamic systems that undergo an impact collision with another dynamic system that is unactuated. This research is specifically focused on a planar robot colliding with a mass-spring system as an academic example of a broader class of such systems. The control objective is defined as the desire to command a planar robot to collide with an unactuated system and regulate the resulting coupled mass-spring robot (MSR) system to a desired compressed state. The collision is modeled as a differentiable impact. Lyapunov-based methods are used to develop a continuous adaptive controller that yields asymptotic regulation of the mass and robot links. A desired time-varying robot link trajectory is designed that accounts for the impact dynamics and the resulting coupled dynamics of the MSR system. The desired link trajectory converges to a setpoint that equals the desired mass position plus an additional constant that is due to the deformation of the mass. A force controller is then designed to ensure that the robot link position tracking error is regulated. Unlike some other results in literature, the continuous force controller does not depend on measuring the impact force or the measurement of other acceleration terms: only the position and velocity terms of the spring-mass system and the joint angles and the angular velocity terms of the planar robotic arm are needed for the proposed controller.

Chapter 2 provides a first step at controlling the proposed impact system. The control development in Chapter 2 is based on the assumption of exact model knowledge of the system dynamics. The controller is proven to regulate the states of a planar robot colliding with the unactuated mass-spring system and yields a global asymptotic regulation result. In Chapter 3, the dynamic model for the systems is assumed to have uncertain parameters. The control objective is defined as the desire to regulate the system to a desired compressed state while compensating for the constant, unknown system parameters. Two linear parameterizations are designed to adapt for the unknown robot and mass-spring parameters. The controller is proven to regulate the states of the systems and yields a global asymptotic regulation result. Another main theme of the impact control is the desire to prescribe, reduce, or control the interaction forces during or after the robot impact with the environment because large interaction forces can damage both the robot and/or the environment or lead to degraded performance or instabilities. In Chapter 4 the feedback elements for the controller of Chapter 3 are contained inside of hyperbolic tangent functions as a means to limit the impact forces resulting from large initial conditions as the robot transitions from non-contact to contact states. The controller yields semi-global asymptotic regulation of the system. Experimental results are provided to illustrate the successful performance of the controller in each chapter.

CHAPTER 1
INTRODUCTION

1.1 Introduction

The problem of controlling a robot during a non-contact to contact transition has been a historically challenging problem that is practically motivated by applications that require a robotic system to interact with the environment. If the contact dynamics are not properly modeled and controlled, the contact forces could result in poor system performance and instabilities. One difficulty in controlling systems subject to non-contact to contact transition is that the dynamics are different when the system status changes suddenly from the non-contact state to a contact state. Another difficulty is measuring the contact force, which can depend on the geometry of the robot, the geometry of the environment, and the type of contact. As stated by Tornambe [10], the appeal of systems with contact conditions is that short-duration effects such as high stresses, rapid dissipation of energy, and fast acceleration and deceleration may be achieved from low-energy sources.

Over the last two decades, many researchers have investigated the modeling and control of contact systems including: [2]-[40]. Two trends are apparent after a comprehensive survey of contact systems in control literature. Most controllers target contacts with a static environment for a fully actuated system. Many researchers also exploit switching or discontinuous controllers to accommodate for the contact conditions. A class of switching controllers were examined by Brogliato et al. in [3] for mechanical systems with differentiable dynamics subject to an algebraic inequality condition and an impact rule relating the interaction impulse and the velocity. The analysis in [3] utilized a discrete Lyapunov function that required the use of the Dini derivative to examine the stability of the system. A

simple mechanical system subject to nonsmooth impacts is considered by Menini and Tornambe [8], where the desired time-varying planar motion of a mass is controlled within a closed region defined by an infinitely massive and rigid circular barrier. In [9], Sekhavat et al. utilized LaSalle's Invariant Set Theorem to prove the stability of a discontinuous controller that is designed to regulate the impact of a hydraulic actuator with a static environment where no knowledge of the impact dynamics is required. The regulation of a one-link robot that undergoes smooth or non-smooth impact dynamics was examined by Tornambe [10]. Volpe and Khosla developed a nonlinear impact control strategy for a robot manipulator experiencing an impact with a static environment [11]. The controller in [11] was based on the concept that negative proportional force gains, or impedance mass ratios less than unity, can provide impact response without bouncing. Tornambe [23] also proposed a switching controller to globally asymptotically regulated a two degree-of-freedom (DOF) planar manipulator to contact an infinitely rigid and massive surface. Pagilla and Yu [24] proposed a discontinuous stable transition controller to deal with the transition from a non-contact to a contact state where explicit knowledge of the impact model is not required. A discontinuous model-based adaptive controller was proposed by Akella et al. [26] to asymptotically stabilize the contact transition between a robot and static environment. Tarn et al. [27] proposed a sensor-referenced control method using positive acceleration feedback with a switching control strategy for impact control for a robot and a constrained surface. A switching controller was also proposed by Wu et al. in [28] to eliminate the bouncing phenomena associated with a robot impacting a static surface. The structure of the switching controller in [28] was dependent on impact feedback from a force sensor. Lee et al. developed a hybrid bang-bang impedance/time-delay controller that establishes a stable interaction between a robot with nonlinear joint friction and a stiff environment in [29] and [30]. Nelson

et al. [31]-[33] proposed a nonlinear control strategy that considers force and vision feedback simultaneously and then switches to pure force control when it is unable to accurately resolve the location of the robot's end-effector relative to the surface to be contact. Motivation exists to explore alternative control strategy for the impact systems because impacts between the robot and the static environment cannot represent all the impact system applications such as the capture of disabled satellites, spaceport docking, manipulation of non-rigid bodies, and so on, and discontinuous controllers require infinite control frequency (i.e., exhibit chattering) or yield degraded stability results (i.e., uniformly ultimately bounded). As stated previously, it is necessary to consider the impact control between two dynamic systems.

Several controllers have been developed for under-actuated dynamic systems that have an impact collision. For example, a family of dead-beat feedback control laws were proposed by Brogliato and Rio [4] to control a class of juggling-like systems. One of the contributions in [4] is a study of the intermediate controllability properties of the object's impact Poincaré mapping. A proportional-derivative (PD) controller was developed by Indri and Tornambe [6] to address global asymptotic stabilization of under-actuated mechanical systems subject to smooth impacts with a static object. In our previous work in [16], a nonlinear energy-based controller is developed to globally asymptotically stabilize a dynamic system subject to impact with a deformable static mass. The contribution in [16] is that the under-actuated states are coupled through the energy of the system as a means to mitigate the transient response of the unactuated states.

This research considers a class of fully actuated dynamic systems that undergo an impact collision with another dynamic system that is unactuated. This research is specifically focused on a planar robot colliding with a mass-spring system as an academic example of a broader class of such systems. The control objective is

defined as the desire to command a planar robot to collide with an unactuated system and regulate the resulting coupled mass-spring robot (MSR) system to a desired compressed state. The collision is modeled as a differentiable impact as in recent work in [6], [10], and our previous efforts in [13]-[16]. Lyapunov-based methods are used to develop a continuous adaptive controller that yields asymptotic regulation of the mass and robot links. A desired time-varying robot link trajectory is designed that accounts for the impact dynamics and the resulting coupled dynamics of the MSR system. The desired link trajectory converges to a setpoint that equals the desired mass position plus an additional constant that is due to the deformation of the mass. A force controller is then designed to ensure that the robot link position tracking error is regulated. Unlike some other results in literature, the continuous force controller does not depend on measuring the impact force or the measurement of other acceleration terms: only the position and velocity terms of the spring-mass system and the joint angles and the angular velocities terms of the planar robotic arm are needed for the proposed controller.

Chapter 2 and our preliminary efforts in [13] provide a first step at controlling the proposed impact system. The control development in Chapter 2 is based on the assumption of exact model knowledge of the system dynamics. The nonlinear continuous Lyapunov-based controller is proven to regulate the states of a planar robot colliding with the unactuated mass-spring system and yields global asymptotic result.

In Chapter 3 and our preliminary results in [14], the dynamic model for the system is assumed to have uncertain parameters. The control objective is defined as the desire to command the planar robot to collide with the mass-spring system and regulate the resulting coupled mass-spring robot (MSR) system to a desired compressed state while compensating for the constant, unknown system parameters. Two linear parameterizations are designed to adapt for the unknown

robot and mass-spring parameters. An adaptive nonlinear continuous Lyapunov-based controller is proven to regulate the states of the systems and yields global asymptotic regulation result.

When the controllers in Chapter 2 and Chapter 3 were implemented in the presence of large initial conditions, violent impacts between the robot and the mass-spring system resulted. In fact, the controller was artificially saturated (the saturation effects were not considered in the stability analysis) to reduce the impact forces so that the mass deflection would not destroy a capacitance probe. Various researchers have investigated methods that prescribe, reduce, or control the interaction forces during or after the robot impact with the environment such as [17]-[40] because large interaction forces can damage both the robot and/or the environment or lead to degraded performance or instabilities. Walker and Gertz et al. exploited kinematic redundancy of the manipulator to reduce the impact force in [19]-[21]. By modeling the impact dynamics as a state dependent jump linear system, Chiu and Lee were able to apply a modified stochastic maximum principle for state dependent jump linear systems to optimize the approach velocity, the force transient during impact and the steady state force error after contact is established [22]. A two degree-of-freedom (DOF) planar manipulator was globally asymptotically regulated to contact an infinitely rigid and massive surface by Tornambe [23] where the impact force was estimated using a reduced-order observer. Pagilla and Yu [24] proposed a stable transition controller to deal with the transition from a non-contact to a contact state which can improve transition performance and force regulation. Hyde and Cutkosky [25] proposed an approach, based on input command shaping, to suppress vibration during the contact transition of switching controllers by modifying feedforward information. A discontinuous model-based adaptive controller was proposed by Akella et al. [26] to asymptotically stabilize the contact transition between a robot and static

environment. The controllers for each contact state were tuned independently to reduce contact force during the process of making contact with the environment. Tarn et al. [27] [28] proposed a sensor-referenced control method using positive acceleration feedback with a switching control strategy for impact control and force regulation for a robot and a constrained surface where the peak impulsive force and bouncing caused directly by overshooting and oscillation of the transient force response can be reduced. Lee et al. developed a hybrid bang-bang impedance/time-delay controller that establishes a stable contact and achieves the desired dynamics for contact or non-contact conditions in [29] and [30], where the force overshoots can be minimized. Nelson et al. [31]-[33] proposed a switching nonlinear controller that combines force and vision control. When the robot's end-effector approaches the target, the controller switches to force control to minimize impact force and to regulate the contact force. Various other applications also focused on the reduction of impact force between different systems during the control process such as impact force reduction of hopping robot considered by Shibata and Natori [34] and Ohnishi et al. [35] [36], bilateral telerobotic system considered by Dubey et al. [37], human-robot symbiotic environment considered by Yamada et al. [38] and Li et al. [39], and space manipulator and free-flying target considered by Huang et al. [40]. Exploring alternative methods is motivated because kinematic redundancy is not always possible, and again the discontinuous controllers require infinite control frequency (i.e., exhibit chattering) or yield degraded stability results (i.e., uniformly ultimately bounded).

These results provide the motivation for the control development in Chapter 4. Specifically, the feedback elements for the continuous controller in Chapter 3 are contained inside of hyperbolic tangent functions as a means to limit the impact forces resulting from large initial conditions as the robot transitions from non-contact to contact states. Although saturating the feedback error is an intuitive

solution that has been proposed in previous literature for other types of robotic systems with limited actuation, several new technical challanges arise due to the impact condition. The main challange is that the use of saturated feedback does not allow some coupling terms to be canceled in the stability analysis, resulting in the need to develop state dependent upper bounds that reduce the stability to a semi-global result (as compared to the global results in Chapter 2 and Chapter 3). The semi-global result is problematic in the current applicative context because certain control terms do not appear in the closed-loop error system during the non-contact condition, resulting in a uniformly ultimately bounded result until the robot makes contact. Hence, the result hinges on new development within the semi-global stability proof for an error system that is only uniformly ultimately bounded during the non-contact phase. This problem is exacerbated by the fact that the Lyapunov function contains radially unbounded hyperbolic functions of some states that only appear inside of saturated hyperbolic terms in the Lyapunov derivative. New control development, closed-loop error systems, and Lyapunov-based stability analysis arguements are used to conclude the result. Experimental results are provided to illustrate the successful performance of the controller in each chapter.

1.2 Dynamic Model

The subsequent development is motivated by the academic problem illustrated in Fig. 1–1. The dynamic model for the two-link revolute robot depicted in Fig. 1–1 can be expressed in the joint-space as

$$M(q)\ddot{q} + C(q,\dot{q})\dot{q} + h(q) = \tau, \tag{1–1}$$

where $q(t), \dot{q}(t), \ddot{q}(t) \in \mathbb{R}^2$ represent the angular position, velocity, and acceleration of the robot links, respectively, $M(q) \in \mathbb{R}^{2\times 2}$ represents the uncertain inertia matrix, $C(q,\dot{q}) \in \mathbb{R}^{2\times 2}$ represents the uncertain centripetal-Coriolis effects, $h(q) \triangleq$

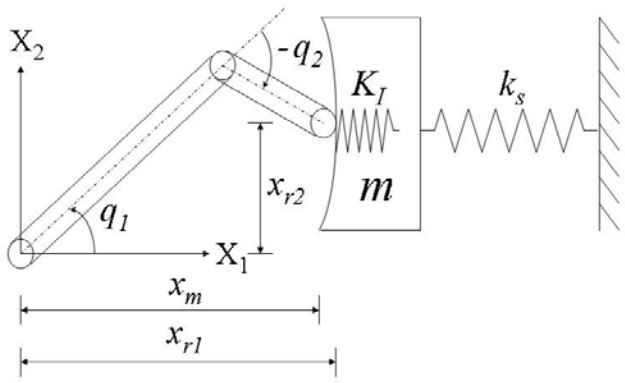

Figure 1–1: The Mass-Spring Robot (MSR) system is an academic example of an impact between two dynamic systems.

$[h_1(q), h_2(q)]^T \in \mathbb{R}^2$ represents uncertain conservative forces (e.g., gravity), and $\tau(t) \in \mathbb{R}^2$ represents the torque control inputs. The Euclidean position of the end-point of the second robot link is denoted by $x_r(t) \triangleq [x_{r1}(t), x_{r2}(t)]^T \in \mathbb{R}^2$, which can be related to the joint-space through the following kinematic relationship:

$$\dot{x}_r = J(q)\dot{q}, \tag{1–2}$$

where $J(q) \in \mathbb{R}^{2\times 2}$ denotes the manipulator Jacobian. The unforced dynamics of the mass-spring system in Fig. 1–1 are

$$m\ddot{x}_m + k_s(x_m - x_0) = 0, \tag{1–3}$$

where $x_m(t), \dot{x}_m(t), \ddot{x}_m(t) \in \mathbb{R}$ represent the displacement, velocity and acceleration of the mass $m \in \mathbb{R}$, $x_0 \in \mathbb{R}$ represents the initial undisturbed position of the mass, and $k_s \in \mathbb{R}$ represents the stiffness of the spring.

Assumption 1.1: We assume that $x_{r1}(t)$ and $x_m(t)$ can be bounded as

$$\zeta_{x_r} \leq x_{r1}(t) \qquad x_m(t) \leq \zeta_{x_m} \tag{1–4}$$

where $\zeta_{x_r} \in \mathbb{R}$ is a known constant that is determined by the minimum coordinate of the robot along the X_1-axis, and $\zeta_{x_m} \in \mathbb{R}$ is a known positive constant. The

lower bound assumption for $x_{r1}(t)$ is based on the geometry of the robot, and the upper bound assumption for $x_m(t)$ is based on the physical fact that the mass is attached by the spring to some object, and the mass will not be able to move past that object.

In the following, the contact model is considered as an elastic contact with finite stiffness. An impact between the second link of the robot and the spring-mass system occurs when $x_{r1}(t) \geq x_m(t)$ (see Fig. 1–1). The impact will yield equal and opposite force reactions between the robot and mass-spring system. Specifically, the impact force acting on the mass, represented by $F_m(x_r, x_m) \in \mathbb{R}$, is assumed to have the following form [6], [10]

$$F_m = K_I \Lambda (x_{r1} - x_m), \tag{1–5}$$

where $K_I \in \mathbb{R}$ represents a positive stiffness constant, and $\Lambda(x_r, x_m) \in \mathbb{R}$ is defined as

$$\Lambda = \begin{cases} 1 & x_{r1} \geq x_m \\ 0 & x_{r1} < x_m. \end{cases} \tag{1–6}$$

The impact force acting on the robot links produces a torque, denoted by $\tau_d(x_r, x_m, q) \in \mathbb{R}^2$, as follows:

$$\tau_d = K_I \Lambda \left(x_{r1} - x_m\right) \begin{bmatrix} l_1 \sin(q_1) + l_2 \sin(q_2 + q_1) \\ l_2 \sin(q_2 + q_1) \end{bmatrix}, \tag{1–7}$$

where $l_1, l_2 \in \mathbb{R}$ denote the robot link lengths. Based on (1–1), (1–3), and (1–5)-(1–7), the dynamic model for the MSR system can be expressed as

$$\begin{aligned} M(q)\ddot{q} + C(q, \dot{q})\dot{q} + h(q) - \tau_d &= \tau \\ m\ddot{x}_m + k_s(x_m - x_0) &= F_m. \end{aligned} \tag{1–8}$$

After premultiplying the robot dynamics by the inverse of the Jacobian transpose and utilizing (1–2), the dynamics in (1–8) can be rewritten as [13], [14]

$$\bar{M}\left(x_r\right)\ddot{x}_r + \bar{C}\left(x_r, \dot{x}_r\right)\dot{x}_r + \bar{h}(x_r) + \begin{bmatrix} F_m \\ 0 \end{bmatrix} = F \tag{1–9}$$

$$m\ddot{x}_m + k_s(x_m - x_0) = F_m, \tag{1–10}$$

where $F(t) \triangleq J^{-T}(q)\tau(t) \in \mathbb{R}^2$ denotes the manipulator force. The dynamic model in (1–9) and (1–10) exhibits the following properties that will be utilized in the subsequent analysis.

Property 1.1: The inertia matrix $\bar{M}(x_r)$ is symmetric, positive definite, and can be lower and upper bounded as

$$a_1||\xi||^2 \leq \xi^T \bar{M}\xi \leq a_2||\xi||^2, \qquad \forall \xi \in \mathbb{R}^2 \tag{1–11}$$

where $a_1, a_2 \in \mathbb{R}$ are positive constants.

Property 1.2: The following skew-symmetric relationship is satisfied

$$\xi^T(\frac{1}{2}\dot{\bar{M}}(x_r) - \bar{C}(x_r, \dot{x}_r))\xi = 0 \qquad \forall \xi \in \mathbb{R}^2. \tag{1–12}$$

CHAPTER 2
LYAPUNOV-BASED CONTROL OF A ROBOT AND MASS-SPRING SYSTEM UNDERGOING AN IMPACT COLLISION

This chapter and our preliminary efforts in [13] provide a first step at controlling the proposed impact system in Section 1.2. The academic example of a planar robot colliding with an unactuated mass-spring system is used to represent a broader class of such systems. The control development in this chapter is based on the assumption of exact model knowledge of the system dynamics. The control objective is to command a robot to collide with an unactuated mass-spring system and regulate the spring-mass to a desired compressed state. Lyapunov-based methods are used to develop a continuous controller that yields global asymptotic regulation of the spring-mass and robot links. Unlike some other results in literature, the developed continuous force controller does not depend on sensing the impact, measuring the impact force, or the measurement of other acceleration terms. Experimental results are provided to validate our analysis.

This chapter is organized as follows. Section 2.1 describes the error system and control development followed by the stability analysis in Section 2.2. Section 2.3 describes the experimental set up and results that indicate the successful performance obtained by implementing the proposed controller followed by conclusion in Section 2.4.

2.1 Error System and Control Development

2.1.1 Control Objective

One goal in this chapter is to regulate the states of a dynamic system (i.e., a two-link planar robot) that has an impact collision with another dynamic system (i.e., a mass-spring). A regulation error, denoted by $e(t) \in \mathbb{R}^3$, is defined to

quantify the control objective as

$$e \triangleq \begin{bmatrix} e_r^T & e_m \end{bmatrix}^T \tag{2–1}$$

where $e_r(t) \triangleq [e_{r1}, e_{r2}]^T \in \mathbb{R}^2$ and $e_m(t) \in \mathbb{R}$ denote the regulation error for the robot and mass-spring system, respectively, and are defined as

$$e_r \triangleq x_{rd} - x_r \qquad e_m \triangleq x_{md} - x_m. \tag{2–2}$$

In (2–2), $x_{md} \in \mathbb{R}$ denotes the constant known desired position of the spring-mass. The desired position of the end-point of the second robot link, denoted by $x_{rd}(t) \triangleq [x_{rd1}, x_{rd2}]^T \in \mathbb{R}^2$, is selected so that the robot will produce the desired spring-mass position while accounting for the impact dynamics. Specifically, $x_{rd1}(t)$ (i.e., the desired horizontal Euclidean coordinate in Fig. 1–1) is a time-varying signal that is subsequently designed to account for the impact condition and the coupled dynamic response of the MSR system, and x_{rd2} (i.e., the desired vertical Euclidean coordinate in Fig. 1–1) is selected as a constant. Filtered tracking errors, denoted by $r_r(t) \in \mathbb{R}^2$ and $r_m(t) \in \mathbb{R}$, are defined as

$$r_r \triangleq \dot{e}_r + \alpha e_r \qquad r_m \triangleq \dot{e}_m + \alpha e_m \tag{2–3}$$

to facilitate the subsequent control design and stability analysis where $\alpha \in \mathbb{R}$ is a positive control parameter.

2.1.2 Closed-Loop Error System

By taking the time derivative of $mr_m(t)$ and utilizing (2–2) and (2–3), the following open-loop error system can be obtained:

$$m\dot{r}_m = k(x_m - x_0) - K\Lambda(x_{r1} - x_m) + \alpha m\dot{e}_m \tag{2–4}$$

where the spring-mass dynamics in (1–10) were substituted for $m\ddot{x}_m(t)$. Motivated to design the desired robot link trajectory to position the spring-mass, (2–2) is used

to rewrite the open-loop system in (2–4) as

$$m\dot{r}_m = k(x_m - x_0) + \alpha m\dot{e}_m + K\Lambda e_{r1} + K\Lambda x_m - K\Lambda x_{rd1}. \tag{2–5}$$

Based on (2–5), the desired robot link position is designed as

$$\begin{aligned} x_{rd1} &\triangleq \frac{1}{K}(\alpha m\dot{e}_m + k(x_m - x_0)) + \frac{1}{K}\left(k_1 + k_2\right) r_m + x_m \\ x_{rd2} &\triangleq \varepsilon \end{aligned} \tag{2–6}$$

where $\varepsilon \in \mathbb{R}$ is an appropriate positive constant (i.e., ε is selected so the robot will impact the mass-spring system), and k_1 and $k_2 \in \mathbb{R}$ are positive constant control gains. After substituting (2–6) into (2–5), the closed-loop error system for $r_m(t)$ can be obtained as

$$m\dot{r}_m = (1 - \Lambda)\left(k(x_m - x_0) + \alpha m\dot{e}_m\right) + K\Lambda e_{r1} - \Lambda\left(k_1 + k_2\right) r_m. \tag{2–7}$$

As $x_m(t) \rightarrow x_{md}$, (2–2) and (2–3) can be used to conclude that $r_m(t) \rightarrow 0$, $\dot{e}_m(t) \rightarrow 0$, and $e_m(t) \rightarrow 0$. Hence, (2–6) can be used to conclude that

$$x_{rd1}(t) \rightarrow \frac{k}{K}(x_m - x_0) + x_{md}. \tag{2–8}$$

The physical meaning of (2–8) is that the desired robot position varies in time to account for the impact dynamics and the coupled dynamic system, and the desired steady-state value is a constant that equals the desired spring-mass position plus the mass deformation.

After taking the time derivative of $r_r(t)$ and premultiplying by the robot inertia matrix, the following open-loop error system is obtained:

$$\bar{M}\dot{r}_r = \bar{M}\ddot{x}_{rd} - F + \bar{C}\dot{x}_r + \bar{h} + \begin{bmatrix} K\Lambda(x_{r1} - x_m) \\ 0 \end{bmatrix} + \alpha\bar{M}\dot{e}_r, \tag{2–9}$$

where (1–10) and (2–2) were utilized. Based on (2–9) and the subsequent stability analysis, the robot force control input is designed as

$$F \triangleq \bar{M}\ddot{x}_{rd} + \bar{C}\dot{x}_{rd} + \bar{h} + \begin{bmatrix} K\Lambda(x_{r1} - x_m) \\ 0 \end{bmatrix} + k_3 r_r + \alpha \left(\bar{M}\dot{e}_r + \bar{C}e_r\right) + e_r, \quad (2\text{–}10)$$

where $k_3 \in \mathbb{R}$ is a positive constant control gain. Based on the use of the backstepping method, the robot force control input in (2–10) requires the first and second derivative of $x_{rd}(t)$. As described in the Appendix A, the first and second derivative of $x_{rd}(t)$ exists (i.e., $x_{rd}(t)$ is continuously differentiable) and do not depend on acceleration terms. The closed-loop error system for $r_r(t)$ can be obtained after substituting (2–10) into (2–9) as

$$\bar{M}\dot{r}_r = -k_3 r_r - \bar{C}r_r - e_r. \quad (2\text{–}11)$$

2.2 Stability Analysis

Theorem: The controller given by (2–10) ensures global asymptotic stability of the robot and spring-mass regulation errors in the sense that

$$|e_m(t)| \to 0 \qquad \|e_r(t)\| \to 0 \quad as \quad t \to \infty \quad (2\text{–}12)$$

provided the following gain condition is satisfied:

$$\alpha > \frac{K^2}{4k_2}. \quad (2\text{–}13)$$

In the following proof, a Lyapunov function and its derivative are provided. The analysis is then separated into two cases: contact and non-contact. For the non-contact case, the stability analysis indicates the controller and error signals are bounded and converge to an arbitrarily small region. Additional analysis indicates that within this region, contact must occur. When contact occurs, a Lyapunov

analysis is provided that illustrates the MSR system asymptotically converges to the desired setpoint.

Proof: Let $V(r_m, r_r, e_r) \in \mathbb{R}$ denote the following continuously differentiable, nonnegative, radially unbounded function (i.e. a Lyapunov function candidate)

$$V \triangleq \frac{1}{2} m r_m^2 + \frac{1}{2} r_r^T \bar{M} r_r + \frac{1}{2} e_r^T e_r. \tag{2–14}$$

The Lyapunov function candidate in (2–14) can be lower and upper bounded as

$$\gamma_1 \|z\|^2 \leq V \leq \gamma_2 \|z\|^2 \tag{2–15}$$

where $\gamma_1, \gamma_2 \in \mathbb{R}$ are positive constants, and $z(t) \in \mathbb{R}^5$ is defined as

$$z(t) \triangleq \begin{bmatrix} r_m & r_r^T & e_r^T \end{bmatrix}^T.$$

The time derivative of (2–14) can be determined as

$$\begin{aligned} \dot{V} = r_m^T((1-\Lambda)\left(k(x_m - x_0) + \alpha m \dot{e}_m\right)) + r_m^T K \Lambda e_{r1} \\ - \Lambda\left(k_1 + k_2\right) r_m^T r_m - k_3 r_r^T r_r - \alpha e_r^T e_r \end{aligned} \tag{2–16}$$

where (1–12), (2–3), (2–7), and (2–11) were utilized. The remainder of the analysis is divided into two cases: Case 1-the robot and mass-spring systems are not in contact (i.e., $x_{r1} < x_m$ and $\Lambda = 0$), and Case 2-the robot and mass-spring systems are in contact (i.e., $x_{r1} \geq x_m$ and $\Lambda = 1$).

Case 1a: Before the initial contact, the mass-spring system is at rest and the spring is not compressed; hence,

$$k(x_m - x_0) = 0 \qquad \dot{e}_m = 0. \tag{2–17}$$

Based on (2–17), (2–16) can be expressed as

$$\dot{V} = -k_3 r_r^T r_r - \alpha e_r^T e_r. \tag{2–18}$$

The expressions in (2–14) and (2–18) can be used to prove that $e_r(t)$, $r_r(t)$, $r_m(t) \in \mathcal{L}_\infty$ and that $e_r(t)$, $r_r(t) \in \mathcal{L}_2$. Based on the fact that $e_r(t)$, $r_r(t)$, $r_m(t) \in \mathcal{L}_\infty$, standard signal chasing arguments can be used to prove that $\dot{e}_r(t)$, $\dot{r}_r(t)$, $x_{rd}(t)$, $F(t) \in \mathcal{L}_\infty$ along with all of the other closed-loop signals. Since $e_r(t)$, $r_r(t) \in \mathcal{L}_\infty \cap \mathcal{L}_2$ and are uniformly continuous, Barbalat's Lemma can be applied to conclude that

$$\|r_r(t)\| \to 0 \qquad \|e_r(t)\| \to 0 \quad as \quad t \to \infty. \tag{2–19}$$

The result in (2–19) can be used along with (2–6) to conclude that

$$x_{rd1}(t) \to \frac{1}{K}(k_1 + k_2)\alpha e_m + x_0$$

leading to an impact with the mass-spring system.

Case 1b: After an impact, the robot may loose contact with the spring-mass. In this case

$$k(x_m - x_0) \neq 0 \qquad \dot{e}_m = -\dot{x}_m. \tag{2–20}$$

Based on (2–20), (2–16) can be expressed as

$$\dot{V} = r_m^T \left(k(x_m - x_0) + \alpha m \dot{e}_m + r_m\right) - k_3 r_r^T r_r - \alpha e_r^T e_r - r_m^T r_m. \tag{2–21}$$

For this case, the initial velocity of the spring-mass is denoted by $\xi \in \mathbb{R}$ and the initial position is denoted by $\bar{x}_m \in \mathbb{R}$. Given the aforementioned initial conditions, the solution for $x_m(t)$ can be obtained from (1–10) as

$$x_m(t) = x_0 + (\bar{x}_m - x_0)\cos(\sqrt{\frac{k}{m}}t) + \xi\sqrt{\frac{m}{k}}\sin(\sqrt{\frac{k}{m}}t). \tag{2–22}$$

The time derivative of (2–22) can be expressed as

$$\dot{x}_m(t) = -(\bar{x}_m - x_0)\sqrt{\frac{k}{m}}\sin(\sqrt{\frac{k}{m}}t) + \xi\cos(\sqrt{\frac{k}{m}}t). \tag{2–23}$$

Based on (2–22) and (2–23), $r_m(t)$ can be expressed as follows:

$$r_m = (\bar{x}_m - x_0)\sqrt{\frac{k}{m}}\sin(\sqrt{\frac{k}{m}}t) - \xi\cos(\sqrt{\frac{k}{m}}t) + \alpha x_{md} - \alpha x_m(t). \tag{2–24}$$

The expressions in (2–22)-(2–24) can be upper bounded as

$$|x_m| \leq |x_0| + |\bar{x}_m - x_0| + |\xi|\sqrt{\frac{m}{k}} \leq \zeta_1 \tag{2–25}$$

$$|\dot{x}_m| \leq |\bar{x}_m - x_0|\left|\sqrt{\frac{k}{m}}\right| + |\xi| \leq \zeta_2 \tag{2–26}$$

$$|r_m| \leq |\bar{x}_m - x_0|\left|\sqrt{\frac{k}{m}}\right| + |\xi| + \alpha\left(x_{md} + \zeta_1\right) \leq \zeta_3 \tag{2–27}$$

where ζ_1, ζ_2, $\zeta_3 \in \mathbb{R}$ denote positive constants. After utilizing (2–25)-(2–27), an upper bound for (2–21) can be developed as

$$\dot{V} \leq -\beta V + \delta \tag{2–28}$$

where $\delta \in \mathbb{R}$ is a positive constant, and $\beta \in \mathbb{R}$ is defined as

$$\beta \triangleq \frac{\min(k_3, \alpha, 1)}{\gamma_2}.$$

Standard techniques can be used to solve (2–28) for $V(t)$ as

$$V(t) \leq \left(V(0) - \frac{\delta}{\beta}\right)\exp(-\beta t) + \frac{\delta}{\beta}. \tag{2–29}$$

Based on (2–29), it is clear that during the transient case (Case 1b) that $e_r(t)$, $r_r(t)$, $r_m(t) \in \mathcal{L}_\infty$. Based on the fact that $e_r(t)$, $r_r(t)$, $r_m(t) \in \mathcal{L}_\infty$, standard signal chasing arguments can be used to prove that $\dot{e}_r(t)$, $\dot{r}_r(t)$, $x_{rd}(t)$, $F(t) \in \mathcal{L}_\infty$ along with all of the other closed-loop signals.

As $\dot{V}(t) \to 0$, eventually $\beta V \leq \delta$. The previous development can be used to conclude that for the non-contact case

$$V \to \frac{\delta}{\beta} \text{ and hence, } \|r_r(t)\|, \|e_r(t)\|, |r_m(t)| \to \frac{\delta}{\beta} \text{ as } t \to \infty. \tag{2–30}$$

Further analysis is required to prove that the manipulator makes contact with the mass-spring system and to achieve the control objective. Contact between the manipulator and the mass-spring system occurs when $x_{r1}(t) \geq x_m(t)$. Based on (2–30), a sufficient condition for contact can be developed as

$$x_{rd1} \geq x_m + \frac{\delta}{\beta}. \tag{2–31}$$

After using (2–6), the sufficient condition in (2–31) can be expressed as

$$\frac{1}{K}(\alpha m \dot{e}_m + k(x_m - x_0)) + \frac{1}{K}(k_1 + k_2) r_m \geq \frac{\delta}{\beta}. \tag{2–32}$$

By using (1–4), (2–3), and (2–30), the inequality in (2–32) can be expressed as

$$\frac{1}{K}(\alpha m(\frac{\delta}{\beta} - \alpha(x_{md} - \zeta_{x_m})) + k(\zeta_{x_m} - x_0)) + \frac{1}{K}(k_1 + k_2)\frac{\delta}{\beta} \geq \frac{\delta}{\beta}. \tag{2–33}$$

Based on (2–33), the control parameter k_1 and k_2 can be selected according to the following sufficient condition to ensure the robot and mass-spring system make contact

$$k_1 + k_2 \geq K - \alpha m + \frac{\alpha^2 \beta m}{\delta}(x_{md} - \zeta_{x_m}) + \frac{\alpha \beta k m}{\delta}(\zeta_{x_m} - x_0). \tag{2–34}$$

Case 2: When the robot and mass-spring systems are in contact, (2–16) can be upper bounded as

$$\dot{V} \leq -k_1 \|r_m\|^2 - k_3 \|r_r\|^2 - \alpha \|e_r\|^2 + [K \|r_m\| \|e_r\| - k_2 \|r_m\|^2]. \tag{2–35}$$

After completing the squares on the bracketed terms, the following expression is obtained:

$$\dot{V} \leq -k_1 \|r_m\|^2 - k_3 \|r_r\|^2 - \left(\alpha - \frac{K^2}{4k_2}\right) \|e_r\|^2. \tag{2–36}$$

Provided the gain condition given in (2–13) is satisfied, (2–15) can be used to upper bound (2–36) as

$$\dot{V} \leq -\gamma_3 V \tag{2–37}$$

where $\gamma_3 \in \mathbb{R}$ is a positive constant. The expression in (2–37) indicates that while in contact, the robot and spring-mass position errors are exponentially regulated, and $e_r(t)$, $r_r(t)$, $r_m(t) \in \mathcal{L}_\infty$. Based on the fact that $e_r(t)$, $r_r(t)$, $r_m(t) \in \mathcal{L}_\infty$, standard signal chasing arguments can be used to prove that $\dot{e}_r(t)$, $\dot{r}_r(t)$, $x_{rd}(t)$, $F(t) \in \mathcal{L}_\infty$ along with all of the other closed-loop signals.

2.3 Experimental Results

The testbed depicted in Fig. 2–1 and Fig. 2–2 was developed for experimental demonstration of the proposed controller. The testbed is composed of a mass-spring system and a two-link robot. The body of the mass-spring system includes a U-shaped aluminum plate (item (8) in Fig. 2–1) mounted on an undercarriage with porous carbon air bearings which enables the undercarriage to glide on an air cushion over a glass covered aluminum rail. A steel core spring (item (1) in Fig. 2–1) connects the undercarriage to an aluminum frame, and a linear variable displacement transducer (LVDT) (item (2) in Fig. 2–1) is used to measure the position of the undercarriage assembly. The impact surface consists of an aluminum plate connected to the undercarriage assembly through a stiff spring mechanism (item (7) in Fig. 2–1). A capacitance probe (item (3) in Fig. 2–1) is used to measure the deflection of the stiff spring mechanism. The two-link robot (items (4-6) in Fig. 2–1) is made of two aluminum links, mounted on 240.0 Nm (base link) and 20.0 Nm (second link) direct-drive switched reluctance motors. The motors are controlled through power electronics operating in torque control mode. The motor resolvers provide rotor position measurements with a resolution of 614400 pulses/revolution, and a standard backwards difference algorithm is used to numerically determine velocity from the encoder readings. A Pentium 2.8 GHz PC operating under QNX hosts the control algorithm, which was implemented via Qmotor 3.0, a graphical user-interface, to facilitate real-time graphing, data logging, and the ability to adjust control gains without recompiling the program

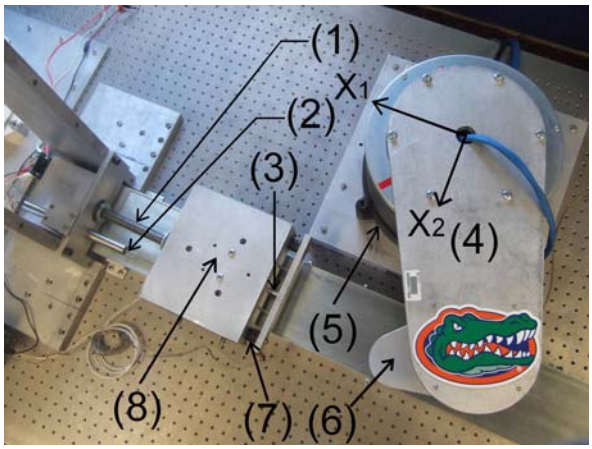

Figure 2–1: Top view of experimental testbed including: (1) mass-spring, (2) LVDT, (3) capacitance probe, (4) link 1, (5) motor 1, (6) link 2, (7) stiff spring mechanism, (8) mass.

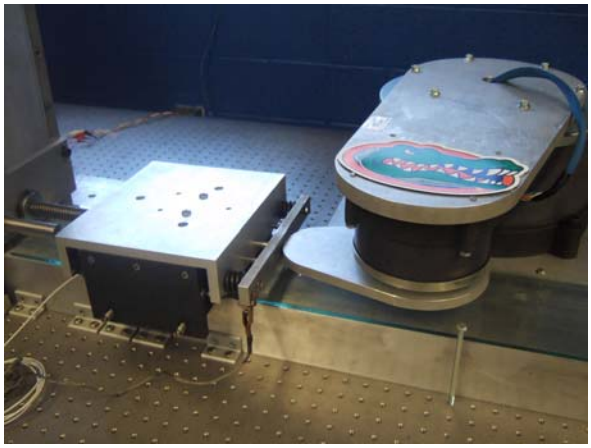

Figure 2–2: Side view of experimental testbed

(for further information on Qmotor 3.0, the reader is referred to [44]). Data acquisition and control implementation were performed at a frequency of 2.0 kHz using the ServoToGo I/O board.

The parameters for the dynamic model in (1–9) and (1–10) have the following values:

$$m_1 = 7.10\ [kg] \quad m_2 = 1.11\ [kg]$$

$$m = 13.6\ [kg] \quad m_s = 10.0\ [kg]$$

$$l_1 = 0.37\ [m] \quad l_2 = 0.17\ [m]$$

$$k = 2000\ [N/m] \quad K = 1.8 \times 10^6\ [N/m]\ ,$$

where m_1, $m_2 \in \mathbb{R}$ represent the mass of the first and second link, $m \in \mathbb{R}$ is the mass of the cart, and $m_s \in \mathbb{R}$ is the mass of the motor that drives the second link. The control gains α and k_3, defined as scalars in (2–3) and (2–10), were implemented (with nonconsequential implications to the stability result) as diagonal gain matrices to provide more flexibility in the experiment. Specifically, the control gains were selected as

$$k_1 = 1 \quad k_2 = 10000 \quad k_3 = diag\{250, 12\} \quad \alpha = diag\{95, 100, 90\}\,.$$

The initial conditions for the robot coordinates and the spring-mass position were (in [m])

$$\begin{bmatrix} x_{r1}(0) & x_{r2}(0) & x_m(0) \end{bmatrix} = \begin{bmatrix} 0.016 & 0.487 & 0.203 \end{bmatrix}.$$

The initial velocity of the robot and spring-mass were zero, and the desired spring-mass position was (in [mm])

$$x_{md} = 233.$$

That is, the tip of the second link of the robot was initially 217 mm from the desired setpoint and 187 mm from impact along the X_1-axis (see Fig. 2–1). Therefore, once the initial impact occurs, the robot is required to depress the spring (item (1) in Fig. 2–1) to move the mass 30 mm along the X_1-axis.

The mass-spring and robot errors (i.e., $e(t)$) are shown in Fig. 2–3. The peak steady-state position error of the robot tip along the X_1-axis (i.e., $|e_{r1}|$) and along the X_2-axis (i.e., $|e_{r2}|$) are 9.6 μm and 92 μm, respectively. The peak steady-state position error of the spring-mass (i.e., $|e_m|$) is 7.7 μm. The 92 μm is due to the lack of the ability of the model to capture friction and slipping effects on the contact surface. In this experiment, a significant friction effect is present along the X_2-axis between the robot tip and the contact surface due to a large normal spring force that is applied along the X_1-axis.

The input control torques (i.e., $J^T(q)F(t)$) are shown in Fig. 2–4 and Fig. 2–5. To constrain the impact force to a level that ensured the aluminum plate did not flex to the point of contact with the capacitance probe, the computed torques are artificially saturated. Fig. 2–4 depicts the computed torques, and Fig. 2–5 depicts the actual torques (solid line) along with the computed torques (dashed line). The resulting desired trajectory along the X_1-axis (i.e., $x_{rd1}(t)$) is depicted in Fig. 2–6, and the desired trajectory along the X_2-axis was chosen as $x_{rd2} = 368$ mm. Fig. 2–7 depicts the value of $\Lambda(x_r, x_m)$ that indicates contact ($\Lambda = 1$) and non-contact ($\Lambda = 0$) conditions for the robot and mass-spring system. A video of the experiment is provided in [45].

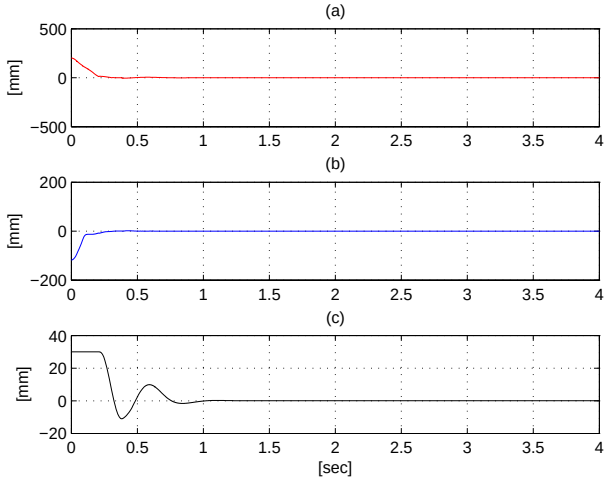

Figure 2–3: The spring-mass and robot errors $e(t)$. Plot (a) indicates the position error of the robot tip along the X_1-axis (i.e., $e_{r1}(t)$), (b) indicates the position error of the robot tip along the X_2-axis (i.e., $e_{r2}(t)$), and (c) indicates the position error of the spring-mass (i.e., $e_m(t)$).

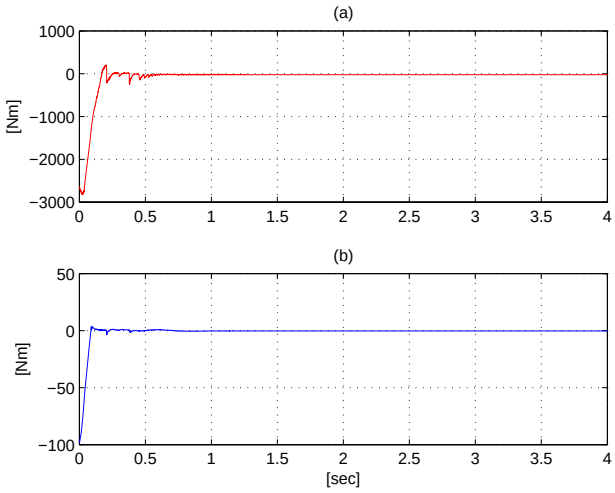

Figure 2–4: Computed control torques $J^T(q)F(t)$ for the (a) base motor and (b) second link motor.

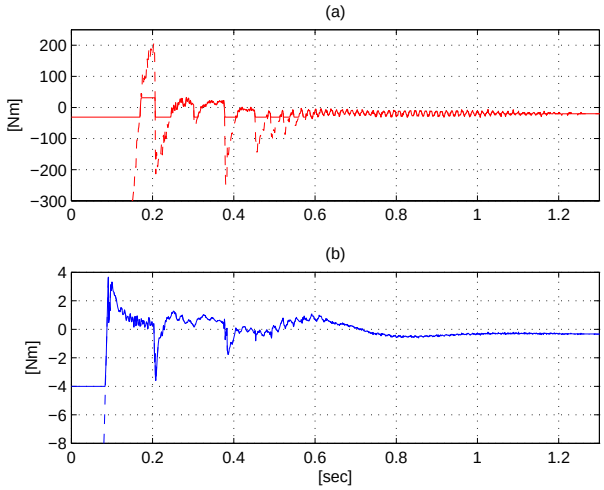

Figure 2–5: Applied control torques $J^T(q)F(t)$ (solid line) versus computed control torques (dashed line) for the (a) base motor and (b) second link motor.

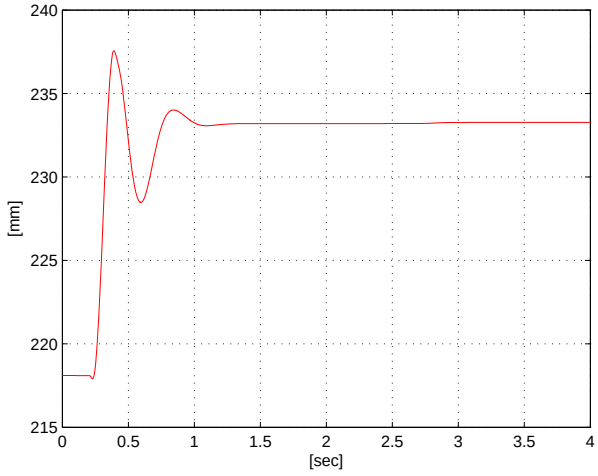

Figure 2–6: Computed desired robot trajectory, $x_{rd1}(t)$.

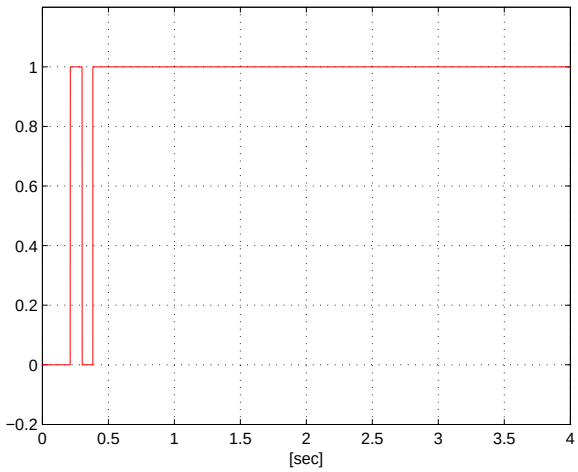

Figure 2–7: Contact ($\Lambda = 1$) and non-contact ($\Lambda = 0$) conditions for the robot and mass-spring system.

2.4 Concluding Remarks

A nonlinear Lyapunov-based controller is proven to regulate the states of a planar robot colliding with an unactuated mass-spring system. The continuous controller yields global asymptotic regulation of the spring-mass and robot links. Unlike some other results in literature, the developed continuous force controller does not depend on sensing the impact, measuring the impact force, or the measurement of other acceleration terms. Innovative analysis methods are used to prove the stability of the system during contact and during different noncontact states. Experimental results are provided to illustrate the successful controller performance.

CHAPTER 3
GLOBAL ADAPTIVE LYAPUNOV-BASED CONTROL OF A ROBOT AND MASS-SPRING SYSTEM UNDERGOING AN IMPACT COLLISION

Similar to Chapter 2, this chapter and our preliminary results in [14] consider a fully actuated planar robot colliding with an unactuated mass-spring system, but unlike Chapter 2 the dynamic model for both the mass-spring and robot systems and the impact force are assumed to have uncertain parameters. The control objective is also defined as the desire to command the robot to collide with an unactuated system and regulate the resulting coupled MSR system to a desired compressed state while compensating for the constant, unknown system parameters. Specifically, in the dynamic model of Section 1.2, $M(q) \in \mathbb{R}^{2\times 2}$ represents the uncertain inertia matrix, $C(q,\dot{q}) \in \mathbb{R}^{2\times 2}$ represents the uncertain centripetal-Coriolis effects, and $h(q) \triangleq [h_1(q), h_2(q)]^T \in \mathbb{R}^2$ represents uncertain conservative forces (e.g., gravity), $m \in \mathbb{R}$ represents the unknown mass and $k_s \in \mathbb{R}$ represents the unknown stiffness of the spring, and $K_I \in \mathbb{R}$ represents the unknown positive stiffness constant.

To compensate for the uncertainty, adaptive Lyapunov-based methods are used to develop a continuous adaptive controller that yields global asymptotic regulation of the mass and robot links. Two linear parameterizations are designed to adapt for the unknown robot and mass parameters. A desired time-varying robot link trajectory is designed that accounts for the impact dynamics and the resulting coupled dynamics of the MSR system. The desired link trajectory converges to a setpoint that equals the desired mass position plus an additional constant that is due to the deformation of the mass. A force controller is then designed to ensure that the robot link position tracking error is regulated.

This chapter is organized as follows. The associated properties and assumptions are provided in Section 3.1. Section 3.2 describes the error system and control development followed by the stability analysis in Section 3.3. Section 3.4 describes the experimental results that indicate the successful performance of the proposed controller followed by conclusion in Section 3.5.

3.1 Properties and Assumptions

Property 3.1: The robot dynamics given in (1–9) can be linearly parameterized as

$$Y(x_r,\ \dot{x}_r,\ \ddot{x}_r)\theta = \bar{M}\left(x_r\right)\ddot{x}_r + \bar{C}\left(x_r, \dot{x}_r\right)\dot{x}_r + \bar{h}(x_r) + \begin{bmatrix} F_m \\ 0 \end{bmatrix},$$

where $\theta \in \mathbb{R}^p$ contains the constant unknown system parameters, and $Y(x_r,\ \dot{x}_r,\ \ddot{x}_r) \in \mathbb{R}^{2\times p}$ denotes the known regression matrix.

Assumption 3.1: We assume that the mass of the mass-spring system can be upper and lower bounded as

$$m_l < m < m_u$$

where $m_l, m_u \in \mathbb{R}$ denote known positive bounding constants. The unknown stiffness constants K_I and k_s are also assumed to be bounded as

$$\underline{\zeta}_K < K_I < \overline{\zeta}_K \qquad \underline{\zeta}_{k_s} < k_s < \overline{\zeta}_{k_s} \tag{3–1}$$

where $\underline{\zeta}_K, \overline{\zeta}_K, \underline{\zeta}_{k_s}, \overline{\zeta}_{k_s} \in \mathbb{R}$ denote known positive bounding constants.

Assumption 3.2: During the subsequent control development, we assume that the minimum singular value of $J(q)$ is greater than a known, small positive constant $\delta > 0$, such that $\max\{\|J^{-1}(q)\|\}$ is known a priori, and hence, all kinematic singularities are always avoided.

3.2 Error System and Control Development

The subsequent control design is based on integrator backstepping methods. A desired trajectory is designed for the robot (i.e., a virtual control input) to ensure the robot converges to and impacts with the mass, and to ensure that the robot regulates the mass to the desired position. Since we can not directly control the robot trajectory, a force controller is developed to ensure that the robot tracks the desired trajectory despite the transition from free motion to an impact collision and despite uncertainties throughout the MSR system. As is typical of the backstepping design method, the derivative of the desired robot trajectory is required to develop the force controller. Taking the derivative of the desired trajectory could lead to unmeasurable higher order terms (i.e., acceleration). The subsequent development exploits the hyperbolic filter structure developed in [42] to overcome the problem of injecting higher order terms in the controller and to facilitate the development of sufficient gain conditions used in the subsequent stability analysis.

3.2.1 Control Objective

The control objective is to regulate the states of an uncertain dynamic system (i.e., a two-link planar robot) that has an impact collision with another uncertain dynamic system (i.e., a mass-spring). A regulation error, denoted by $e(t) \in \mathbb{R}^3$, is defined to quantify this objective as

$$e \triangleq \begin{bmatrix} e_m & e_r^T \end{bmatrix}^T,$$

where $e_r(t) \triangleq [e_{r1}, e_{r2}]^T \in \mathbb{R}^2$ and $e_m(t) \in \mathbb{R}$ denote the regulation error for the end-point of the second link of the robot and mass-spring system (see Fig. 1–1), respectively, and are defined as

$$e_r \triangleq x_{rd} - x_r \qquad e_m \triangleq x_{md} - x_m. \tag{3–2}$$

In (3–2), $x_{md} \in \mathbb{R}$ denotes the constant known desired position of the mass, and $x_{rd}(t) \triangleq [x_{rd1}(t), x_{rd2}]^T \in \mathbb{R}^2$ denotes the desired position of the end-point of the second link of the robot. The subsequent development is based on the assumption that $q(t)$, $\dot{q}(t)$, $x_m(t)$, and $\dot{x}_m(t)$ are measurable, and that $x_r(t)$ and $\dot{x}_r(t)$ can be obtained from $q(t)$ and $\dot{q}(t)$. To facilitate the subsequent control design and stability analysis, filtered tracking errors, denoted by $\eta_m(t) \in \mathbb{R}$ and $r_r(t) \in \mathbb{R}^2$, are defined as [42]

$$\begin{aligned} \eta_m &\triangleq \dot{e}_m + \alpha_1 \tanh(e_m) + \alpha_2 \tanh(e_f) \\ r_r &\triangleq \dot{e}_r + \alpha e_r, \end{aligned} \tag{3–3}$$

where α, α_1, $\alpha_2 \in \mathbb{R}$ are positive, constant gains, and $e_f(t) \in \mathbb{R}$ is an auxiliary filter variable designed as [42]

$$\dot{e}_f \triangleq -\alpha_3 \tanh(e_f) + \alpha_2 \tanh(e_m) - k_1 \cosh^2(e_f)\eta_m, \tag{3–4}$$

where $k_1 \in \mathbb{R}$ is a positive constant control gain, and $\alpha_3 \in \mathbb{R}$ is a positive constant filter gain.

3.2.2 Closed-Loop Error System

By taking the time derivative of $m\eta_m(t)$ and utilizing (1–5), (1–10), (3–2), and (3–3), the following open-loop error system can be obtained:

$$m\dot{\eta}_m = Y_d\theta_d - K_I\Lambda\left(x_{r1} - x_m\right) + \alpha_2 m \cosh^{-2}(e_f)\dot{e}_f + \alpha_1 m \cosh^{-2}(e_m)\dot{e}_m. \tag{3–5}$$

In (3–5), $Y_d(x_m) \triangleq (x_m - x_o)$ and $\theta_d \triangleq k_s$. To facilitate the subsequent analysis, the following notation is introduced [42]:

$$\begin{aligned} Y_d\theta_d &= Y_d K_I K_I^{-1}\theta_d = Y_{dk}\theta_{dk} \\ &= K_I\left(x_m - x_o\right)\left[\frac{k_s}{K_I}\right]. \end{aligned} \tag{3–6}$$

After using (3–3) and (3–4), the expression in (3–5) can be rewritten as

$$m\dot{\eta}_m = Y_d\theta_d + K_I\left(x_{rd1} - \Lambda x_{r1}\right) + K_I\Lambda x_m - K_I x_{rd1} + \chi - \alpha_2 m k_1 \eta_m, \tag{3–7}$$

where $\chi(e_m,\, e_f,\, \eta_m,\, t) \in \mathbb{R}$ is an auxiliary term defined as

$$\begin{aligned}\chi = {} & \alpha_1 m \cosh^{-2}(e_m)\left(\eta_m - \alpha_1 \tanh(e_m)\right) - \alpha_1\alpha_2 m \cosh^{-2}(e_m)\tanh(e_f) \\ & + \alpha_2 m \cosh^{-2}(e_f)\left(-\alpha_3 \tanh(e_f)\right) + \alpha_2 m \cosh^{-2}(e_f)\left(\alpha_2 \tanh(e_m)\right).\end{aligned} \tag{3–8}$$

The auxiliary expression $\chi(e_m,\, e_f,\, \eta_m,\, t)$ defined in (3–8) can be upper bounded as

$$|\chi| \leq \zeta_1 \left\|z\right\|, \tag{3–9}$$

where $\zeta_1 \in \mathbb{R}$ is a positive bounding constant, and $z(t) \in \mathbb{R}^3$ is defined as

$$z = \begin{bmatrix} \eta_m & \tanh(e_m) & \tanh(e_f) \end{bmatrix}. \tag{3–10}$$

Based on (3–7) and the subsequent stability analysis, the desired robot link position is designed as

$$\begin{aligned} x_{rd1} &\triangleq Y_d\hat{\theta}_{dk} + x_m + k_2\tanh(e_m) - k_1 k_2 \cosh^2(e_f)\tanh(e_f) \\ x_{rd2} &\triangleq \varepsilon. \end{aligned} \tag{3–11}$$

In (3–11), $\varepsilon \in \mathbb{R}$ is an appropriate positive constant (i.e., ε is selected so the robot will impact the mass-spring system in the vertical direction), $k_2 \in \mathbb{R}$ is a positive constant control gain, and the control gain $k_1 \in \mathbb{R}$ is defined as

$$k_1 \triangleq \frac{1}{m_l}\left(3 + k_{n1}\zeta_1^2\right), \tag{3–12}$$

where $k_{n1} \in \mathbb{R}$ is a positive constant nonlinear damping gain. The parameter estimate $\hat{\theta}_{dk}(t) \in \mathbb{R}$ in (3–11) is generated by the adaptive update law

$$\dot{\hat{\theta}}_{dk} \triangleq proj(\Gamma Y_d \eta_m). \tag{3–13}$$

In (3–13), $\Gamma \in \mathbb{R}$ is a positive constant, and $proj(\cdot)$ denotes a sufficiently smooth projection algorithm [43] utilized to guarantee that $\hat{\theta}_{dk}(t)$ can be bounded as

$$\underline{\theta}_{dk} \leq \hat{\theta}_{dk} \leq \bar{\theta}_{dk}, \tag{3–14}$$

where $\underline{\theta}_{dk}$, $\bar{\theta}_{dk} \in \mathbb{R}$ denote known, constant lower and upper bounds for $\theta_{dk}(t)$, respectively.

After substituting (3–11) into (3–7), the closed-loop error system for $\eta_m(t)$ can be obtained as

$$\begin{aligned} m\dot{\eta}_m = {} & K_I \left(x_{rd1} - \Lambda x_{r1}\right) + K_I \left(\Lambda x_m - x_m\right) + K_I k_1 k_2 \cosh^2(e_f) \tanh(e_f) \\ & + Y_{dk}\tilde{\theta}_{dk} - K_I k_2 \tanh(e_m) + \chi - \alpha_2 m k_1 \eta_m. \end{aligned} \tag{3–15}$$

In (3–15), the parameter estimation error $\tilde{\theta}_{dk}(t) \in \mathbb{R}$ is defined as

$$\tilde{\theta}_{dk} \triangleq \theta_{dk} - \hat{\theta}_{dk}.$$

The open-loop robot error system can be obtained by taking the time derivative of $r_r(t)$ and premultiplying by the robot inertia matrix as

$$\bar{M}\dot{r}_r = Y_r\theta_r - \bar{C}r_r - F, \tag{3–16}$$

where (1–9), (3–2), and (3–3) were utilized, and

$$Y_r\theta_r = \bar{M}\ddot{x}_{rd} + \alpha\bar{M}\dot{e}_r + \bar{h} + \bar{C}\dot{x}_{rd} + \alpha\bar{C}x_{rd} + \begin{bmatrix} K_I\Lambda(x_{r1} - x_m) \\ 0 \end{bmatrix} - \alpha\bar{C}x_r, \tag{3–17}$$

where $Y_r(x_r, \dot{x}_r, x_m, \dot{x}_m, e_f, \eta_m, t) \in \mathbb{R}^{2\times P}$ denotes a known regression matrix, and $\theta_r \in \mathbb{R}^P$denotes an unknown constant parameter vector. See Appendix A for a linearly parameterizable expression for $\bar{M}\left(x_r\right)\ddot{x}_{rd}(t)$ that does not depend on acceleration terms. Based on (3–16) and the subsequent stability analysis, the robot force

control input is designed as

$$F \triangleq Y_r\hat{\theta}_r + e_r + k_3 r_r, \tag{3–18}$$

where $k_3 \in \mathbb{R}$ is a positive constant control gain, and $\hat{\theta}_r(t) \in \mathbb{R}^P$ is an estimate for θ_r generated by the following adaptive update law

$$\dot{\hat{\theta}}_r \triangleq proj(\Gamma_r Y_r^T r_r). \tag{3–19}$$

In (3–19), $\Gamma_r \in \mathbb{R}^{P\times P}$ is a positive definite, constant, diagonal, adaptation gain matrix, and $proj(\cdot)$ denotes a projection algorithm utilized to guarantee that the $i-th$ element of $\hat{\theta}_r(t)$ can be bounded as

$$\underline{\theta}_{ri} \leq \hat{\theta}_{ri} \leq \bar{\theta}_{ri},$$

where $\underline{\theta}_{ri}$, $\bar{\theta}_{ri} \in \mathbb{R}$ denote known, constant lower and upper bounds for each element of $\theta_r(t)$, respectively.

The closed-loop error system for $r_r(t)$ can be obtained after substituting (3–18) into (3–16) as

$$\bar{M}\dot{r}_r = Y_r\tilde{\theta}_r - k_3 r_r - \bar{C} r_r - e_r. \tag{3–20}$$

In (3–20), the parameter estimation error $\tilde{\theta}_r(t) \in \mathbb{R}^P$ is defined as

$$\tilde{\theta}_r \triangleq \theta_r - \hat{\theta}_r. \tag{3–21}$$

Remark 3.1: Based on (3–18), the control torque input can be expressed as

$$\tau = J^T\left(Y_r\hat{\theta}_r + e_r + k_3 r_r\right) \tag{3–22}$$

where $J(q)$ denotes the manipulator Jacobian introduced in (1–2).

3.3 Stability Analysis

Theorem: The controller given by (3–11), (3–13), (3–18), and (3–19) ensures global asymptotic regulation of the MSR system in the sense that

$$|e_m(t)| \to 0 \qquad \|e_r(t)\| \to 0 \quad as \quad t \to \infty$$

provided k_1, k_2, and k_{n1} are selected sufficiently large and the following sufficient gain condition is satisfied:

$$\alpha_2 > \max\left\{\frac{1}{\alpha}, (\zeta_{x_m} + |\zeta_{x_r}|)^2\right\} \frac{\overline{\zeta}_K^2}{4} \tag{3–23}$$

where ζ_{x_m}, ζ_{x_r}, $\overline{\zeta}_K$, and α are defined in (1–4) and (3–1), respectively.

In the following proof, a Lyapunov function and its derivative are provided. The analysis is then separated into two cases as in Chapter 2. For the non-contact case, the stability analysis indicates the controller and error signals are bounded and converge to an arbitrarily small region. Additional analysis indicates that within this region, contact must occur. When contact occurs, a Lyapunov analysis is provided that illustrates the MSR system asymptotically converges to the desired setpoint.

Proof: Let $V(r_r, e_r, e_m, e_f, \eta_m, \tilde{\theta}_r, \tilde{\theta}_{dk}, t) \in \mathbb{R}$ denote the following nonnegative, radially unbounded function (i.e. a Lyapunov function candidate):

$$\begin{aligned} V \triangleq \frac{1}{2} r_r^T \bar{M} r_r + \frac{1}{2} \tilde{\theta}_r^T \Gamma_r^{-1} \tilde{\theta}_r + \frac{1}{2} \tilde{\theta}_{dk}^T K_I \Gamma^{-1} \tilde{\theta}_{dk} \\ + k_2 K_I \left[\ln\left(\cosh(e_m)\right) + \ln\left(\cosh\left(e_f\right)\right)\right] + \frac{1}{2} e_r^T e_r + \frac{1}{2} m \eta_m^2. \end{aligned} \tag{3–24}$$

The time derivative of (3–24) can be determined as

$$\begin{aligned} \dot{V} = r_r^T \bar{M} \dot{r}_r + \frac{1}{2} r_r^T \dot{\bar{M}} r_r + \tilde{\theta}_r^T \Gamma_r^{-1} \dot{\tilde{\theta}}_r + \tilde{\theta}_{dk}^T K_I \Gamma^{-1} \dot{\tilde{\theta}}_{dk} \\ + k_2 K_I \left[\tanh(e_m)\dot{e}_m + \tanh(e_f)\dot{e}_f\right] + e_r^T \dot{e}_r + \eta_m m \dot{\eta}_m. \end{aligned} \tag{3–25}$$

After using (1–12), (3–3), (3–4), (3–12), (3–13), (3–15), and (3–19)-(3–21), the expression in (3–25) can be rewritten as

$$\dot{V} \leq -k_3 r_r^T r_r - \alpha_1 k_2 K_I \tanh^2(e_m) - 3\alpha_2 \eta_m^2 - k_2 K_I \alpha_3 \tanh^2(e_f) \tag{3–26}$$
$$- k_{n1}\zeta_1^2 \alpha_2 \eta_m^2 - \alpha e_r^T e_r + \eta_m \left[K_I \left(x_{rd1} - \Lambda x_{r1}\right) + K_I \left(\Lambda x_m - x_m\right) + \chi\right].$$

The expression in (3–26) will now be examined under two different scenarios.

Case 1-Non-contact: For this case, the systems are not in contact ($\Lambda = 0$) and (3–26) can be rewritten as

$$\dot{V} \leq -k_3 r_r^T r_r - \alpha_1 k_2 K_I \tanh^2(e_m) - k_2 K_I \alpha_3 \tanh^2(e_f) - 3\alpha_2 \eta_m^2$$
$$- k_{n1}\zeta_1^2 \alpha_2 \eta_m^2 - \alpha e_r^T e_r + \eta_m \left[K_I x_{rd1} - K_I x_m + \chi\right].$$

Rewriting $x_{rd1}(t)$ and substituting for $\chi(e_m,\, e_f,\, \eta_m,\, t)$ yields

$$\dot{V} \leq -k_3 r_r^T r_r - \alpha_1 k_2 K_I \tanh^2(e_m) - k_2 K_I \alpha_3 \tanh^2(e_f) - 2\alpha_2 \eta_m^2 \tag{3–27}$$
$$- \left[\alpha \left\|e_r\right\|^2 - \overline{\zeta}_K \left|\eta_m\right| \left\|e_r\right\|\right] - \left[k_{n1}\alpha_2 \zeta_1^2 \eta_m^2 - \zeta_1 \left\|z\right\| \left|\eta_m\right|\right]$$
$$- \left[\alpha_2 \eta_m^2 - \overline{\zeta}_K \left|\eta_m\right| \left|x_m - x_{r1}\right|\right].$$

After completing the square on the bracketed terms, (3–27) can be expressed as

$$\dot{V} \leq -k_3 r_r^T r_r - \alpha_1 k_2 K_I \tanh^2(e_m) - k_2 K_I \alpha_3 \tanh^2(e_f) - \alpha_2 \eta_m^2 \tag{3–28}$$
$$- \left(\alpha_2 - \frac{\overline{\zeta}_K^2}{4\alpha}\right) \eta_m^2 + \frac{\left\|z\right\|^2}{4\alpha_2 k_{n1}} + \frac{\overline{\zeta}_K^2 \left(x_m - x_{r1}\right)^2}{4\alpha_2}.$$

Provided k_{n1} is selected according to the sufficient condition

$$k_{n1} > \frac{1}{4\alpha_2 \min\left\{\alpha_1 k_2 \underline{\zeta}_K,\ k_2 \underline{\zeta}_K \alpha_3,\ \alpha_2\right\}},$$

the expression in (3–28) can be further reduced as

$$\dot{V} \leq -\lambda_1 \left\|z\right\|^2 - k_3 \left\|r_r\right\|^2 - \left(\alpha_2 - \frac{\overline{\zeta}_K^2}{4\alpha}\right) \eta_m^2 + \frac{\overline{\zeta}_K^2 \left(x_m - x_{r1}\right)^2}{4\alpha_2}, \tag{3–29}$$

where $\lambda_1 \in \mathbb{R}$ is defined as

$$\lambda_1 = \min\left\{\alpha_1 k_2 \underline{\zeta}_K,\ k_2 \underline{\zeta}_K \alpha_3,\ \alpha_2\right\} - \frac{1}{4\alpha_2 k_{n1}}.$$

Based on (1–4) in Assumption 1.1, for the non-contact case

$$\zeta_{x_r} \leq x_{r1} \leq x_m \leq \zeta_{x_m}. \tag{3–30}$$

Hence, the expression in (3–29) can be upper bounded as

$$\dot{V} \leq -\lambda \|y\|^2 + \varepsilon_x \tag{3–31}$$

where $\lambda \in \mathbb{R}$ is defined as

$$\lambda = \min\left\{\lambda_1,\ k_3,\ \left(\alpha_2 - \frac{\overline{\zeta}_K^2}{4\alpha}\right)\right\},$$

and $y(t) \in \mathbb{R}^5$ and $\varepsilon_x \in \mathbb{R}$ are defined as

$$y = \begin{bmatrix} z^T & r_r^T \end{bmatrix}^T \qquad \varepsilon_x = \frac{\overline{\zeta}_K^2 \left(\zeta_{x_m} + |\zeta_{x_r}|\right)^2}{4\alpha_2} \tag{3–32}$$

where ε_x can be made arbitrarily small by making α_2 large. Based on (3–24) and (3–31), either $\lambda \|y\|^2 \leq \varepsilon_x$ or $\lambda \|y\|^2 > \varepsilon_x$. If $\lambda \|y\|^2 > \varepsilon_x$, then Barbalat's Lemma can be used to conclude that $\dot{V}(t) \to 0$ since $V(t)$ is lower bounded, $\dot{V}(t)$ is negative semi-definite, and $\dot{V}(t)$ can be shown to be uniformly continuous. As $\dot{V}(t) \to 0$, eventually $\lambda \|y\|^2 \leq \varepsilon_x$. Provided the sufficient gain condition in (3–23) is satisfied (i.e., $\varepsilon_x < 1$), then (3–10), (3–32), and the facts that $\tilde{\theta}_r(t)$ and $\tilde{\theta}_{dk}(t) \in \mathcal{L}_\infty$ from the use of a projection algorithm, can be used to conclude that $V(\cdot) \in \mathcal{L}_\infty$; hence, $\|y(t)\|$, $\|z(t)\|$, $\|r_r(t)\|$, $\|e_r(t)\|$, $\eta_m(t)$, $e_f(t)$, $e_m(t) \in \mathcal{L}_\infty$. Signal chasing arguments can be used to prove the remaining closed-loop signals are also bounded during the non-contact case. The previous development can be used to conclude

that for the non-contact case

$$\|y(t)\| \to \sqrt{\frac{\varepsilon_x}{\lambda}} \text{ and hence, } \|r_r(t)\| \to \sqrt{\frac{\varepsilon_x}{\lambda}} \text{ as } t \to \infty. \tag{3–33}$$

Based on (3–33), linear analysis methods (see Lemma A.19 of [41]) can be applied to (3–3) to prove that

$$\|e_r(t)\| \to \|e_r(0)\| \exp(-\alpha t) + \frac{1}{\alpha}\sqrt{\frac{\varepsilon_x}{\lambda}} \left(1 - \exp(-\alpha t)\right) \tag{3–34}$$

as $t \to \infty$ for the non-contact case.

Further analysis is required to prove that the manipulator makes contact with the mass-spring system and to achieve the control objective. Contact between the manipulator and the mass-spring system occurs when $x_{r1}(t) \geq x_m(t)$. Based on (3–34), a sufficient condition for contact can be developed as

$$x_{rd1} \geq x_m + \frac{1}{\alpha}\sqrt{\frac{\varepsilon_x}{\lambda}}. \tag{3–35}$$

After using (3–11), the sufficient condition in (3–35) can be expressed as

$$Y_d \hat{\theta}_{dk} + k_2 \tanh(e_m) - k_1 k_2 \cosh^2(e_f) \tanh(e_f) \geq \frac{1}{\alpha}\sqrt{\frac{\varepsilon_x}{\lambda}}. \tag{3–36}$$

By using (3–2) and (3–6) and performing some algebraic manipulation, the inequality in (3–36) can be expressed as

$$k_2 \tanh(e_m) - k_1 k_2 \cosh^2(e_f) \geq \frac{1}{\alpha}\sqrt{\frac{\varepsilon_x}{\lambda}} - x_{md}\underline{\theta}_{dk} + (e_m + x_0)\,\overline{\theta}_{dk} \tag{3–37}$$

where $\overline{\theta}_{dk}(t)$ and $\underline{\theta}_{dk}(t)$ are defined in (3–14). From Assumption 1.1, $e_m(t)$ can be upper bounded as

$$e_m \leq \overline{\varepsilon}_m \tag{3–38}$$

where $\overline{\varepsilon}_m \in \mathbb{R}$ denotes a known positive constant. If $e_m(t) \leq 0$, then the sufficient condition in (3–37) may not be satisfied. The condition that $e_m(t) \leq 0$ will only occur if an impact collision occurs that causes the mass to overshoot the desired

position. However, even if an impact occurs and the mass overshoots the desired position, the dynamics will force the mass position error to return to the initial condition. That is, $e_m(t) \rightarrow x_{md} - x_0 > \underline{\varepsilon}_m$ where $\underline{\varepsilon}_m \in \mathbb{R}$ denotes a known positive constant. Based on (3–38) and the fact that $e_m(t)$ will eventually be lower bounded by $\underline{\varepsilon}_m$ in a noncontact condition, the inequality in (3–37) can be simplified as

$$k_2 \left(\tanh(\underline{\varepsilon}_m) - k_1 \cosh^2(e_f) \right) \geq \frac{1}{\alpha} \sqrt{\frac{\varepsilon_x}{\lambda}} - x_{md} \underline{\theta}_{dk} + (\overline{\varepsilon}_m + x_0) \overline{\theta}_{dk}. \tag{3–39}$$

To further simplify the inequality in (3–39), an upper bound can be determined for $e_f(t)$. The inequality in (3–33) along with (3–10) and (3–32) can be used to conclude that as the manipulator approaches the mass, $e_f(t)$ will eventually be upper bounded as

$$e_f \leq \tanh^{-1} \left(\frac{1}{\alpha} \sqrt{\frac{\varepsilon_x}{\lambda}} \right) \leq \varepsilon_f, \tag{3–40}$$

where $\varepsilon_f \in \mathbb{R}$ is a known positive constant. Based on (3–32) and (3–40), the control parameter k_2 can be selected according to the following sufficient condition to ensure the robot and mass-spring system make contact

$$k_2 \geq \frac{\frac{1}{\alpha} \sqrt{\frac{\varepsilon_x}{\lambda}} - x_{md} \underline{\theta}_{dk} + (\overline{\varepsilon}_m + x_0) \overline{\theta}_{dk}}{\tanh(\underline{\varepsilon}_m) - k_1 \cosh^2(\varepsilon_f)} \tag{3–41}$$

where k_1 is chosen as

$$k_1 < \frac{\tanh(\underline{\varepsilon}_m)}{\cosh^2(\varepsilon_f)}.$$

Case 2-Contact: Provided the sufficient condition in (3–41) is satisfied, the robot will eventually make contact with the mass. For the case when the dynamic systems collide ($\Lambda = 1$), and the two dynamic systems become coupled[1] , then

[1] The dynamic systems can separate after impact, however this case can still be analyzed under the Non-contact section of the stability analysis.

(3–26) can be rewritten as

$$\dot{V} \leq -k_3 r_r^T r_r - \alpha_1 k_2 K_I \tanh^2(e_m) - 3\alpha_2 \eta_m^2 - k_2 K_I \alpha_3 \tanh^2(e_f)$$
$$- \left[\alpha \|e_r\|^2 - \overline{\zeta}_K |\eta_m| \|e_r\|\right] - \left[k_{n1}\zeta_1^2 \alpha_2 \eta_m^2 - \zeta_1 \|z\| |\eta_m|\right],$$

where (3–9) was substituted for $\chi(e_m, e_f, \eta_m, t)$. Completing the square on the two bracketed terms yields

$$\dot{V} \leq -k_3 r_r^T r_r - \alpha_1 k_2 \underline{\zeta}_K \tanh^2(e_m) - \alpha_3 k_2 \underline{\zeta}_K \tanh^2(e_f) \tag{3–42}$$
$$- 3\alpha_2 \eta_m^2 + \frac{\overline{\zeta}_K^2 \eta_m^2}{4\alpha} + \frac{\|z\|^2}{4\alpha_2 k_{n1}}.$$

A final bound can be placed on (3–42) as

$$\dot{V} \leq -\min\left\{\alpha_1 k_2 \underline{\zeta}_K,\ \alpha_3 k_2 \underline{\zeta}_K,\ \alpha_2\right\} \|z\|^2 + \frac{\|z\|^2}{4\alpha_2 k_{n1}} - \left(2\alpha_2 - \frac{\overline{\zeta}_K^2}{4\alpha}\right) \eta_m^2 - k_3 r_r^T r_r.$$

Because (3–24) is non-negative and its derivative is negative semi-definite, $r_r(t)$, $\tilde{\theta}_r(t)$, $\tilde{\theta}_{dk}(t)$, $e_r(t)$, $e_m(t)$, $e_f(t)$, and $\eta_m(t) \in \mathcal{L}_\infty$. Due to the fact that $e_m(t)$, $e_f(t)$, and $\eta_m(t) \in \mathcal{L}_\infty$, the expression in (3–3) can be used to conclude that $\dot{e}_m(t) \in \mathcal{L}_\infty$ (and hence, $e_m(t)$ is uniformly continuous). Due to the fact that $e_m(t) \in \mathcal{L}_\infty$, (3–2) can be used to conclude that $x_m(t) \in \mathcal{L}_\infty$. Previous facts can be used to prove that $x_{rd}(t) \in \mathcal{L}_\infty$, and since $e_r(t) \in \mathcal{L}_\infty$, then $x_r(t) \in \mathcal{L}_\infty$. Due to the fact that $e_f(t)$, $e_m(t)$, $\eta_m(t) \in \mathcal{L}_\infty$, (3–4) can be used to conclude that $\dot{e}_f(t) \in \mathcal{L}_\infty$. The expression in (3–5) can be used to conclude that $\dot{\eta}_m(t) \in \mathcal{L}_\infty$ (and hence, $\eta_m(t)$ is uniformly continuous). Given that $r_r(t)$, $e_m(t)$, $e_f(t)$, and $\eta_m(t) \in \mathcal{L}_\infty$, $Y_r(\cdot) \in \mathcal{L}_\infty$. Since $\tilde{\theta}_r(t) \in \mathcal{L}_\infty$, (3–21) can be used to prove that $\hat{\theta}_r(t) \in \mathcal{L}_\infty$. The expression in (3–18) can then be used to prove that $F(t) \in \mathcal{L}_\infty$. The expression in (3–20) can be used to conclude that $\dot{r}_r(t) \in \mathcal{L}_\infty$ (and hence, $r_r(t)$ is uniformly continuous). Due to the fact that $e_m(t)$, $r_r(t)$, $\eta_m(t) \in \mathcal{L}_2$ and uniformly continuous, Barbalat's Lemma can be used to conclude that $|e_m(t)|$, $\|r_r(t)\|$, $|\eta_m(t)| \to 0$ as $t \to \infty$. Based on the fact that $\|r_r(t)\| \to 0$ as $t \to \infty$,

standard linear analysis methods (see Lemma A.15 of [41]) can then be used to prove that $\|e_r(t)\| \to 0 \quad \text{as} \quad t \to \infty$.

As is typical in literature, the controller developed in (3–11), (3–13), (3–18), and (3–19) is based on the underlying assumption that an arbitrarily large (but finite) control authority is available. A potential disadvantage of the controller is that the gain conditions developed above and in (3–23) indicate that k_{n1}, k_2, and α_2, respectively, should be selected sufficiently large. As demonstrated by the subsequent experimental results, the gains may be selected much lower in practice (i.e., the gains conditions are the result of a conservative Lyapunov analysis). However, the subsequent experimental section also illustrates that even when the gain conditions are violated, large initial conditions and a high stiffness coefficient result in a high gain controller that initially saturates the actuators. The control torque in the experiment was artificially saturated to reduce the magnitude of the impact to protect a capacitance probe from contact by excessive bending of the aluminum rod/spring assembly. Research that can limit the required control torque for systems that undergo an impact collision will be discussed in Chapter 4.

3.4 Experimental Results

With the testbed in Section 2.3, the control gains α and k_3, defined as scalars in (3–3) and (3–18), were implemented (with nonconsequential implications to the stability result) as diagonal gain matrices to provide more flexibility in the experiment. Specifically, the control gains were selected as

$$\begin{gathered} k_1 = 0.18 \quad k_2 = 0.9 \quad k_3 = diag\left\{185, 170\right\} \\ \alpha_1 = 45 \quad \alpha_2 = 8 \quad \alpha_3 = 0.01 \quad \alpha = diag\left\{60, 90\right\}. \end{gathered} \tag{3–43}$$

The control gains in (3–43) were obtained from a trial and error process and may not satisfy the sufficient gain conditions developed in the theorem proof. The sufficient gain conditions are the result of a conservative stability analysis and were

used as a guide in the tuning process. The subsequent results indicate that the developed controller can be applied despite the fact that some gain conditions are not satisfied.

The adaptation gains were selected as

$$\Gamma = 90$$
$$\Gamma_r = diag\{4.01 \times 10^{12}, 1.2 \times 10^{7}, 0.2, 3.3 \times 10^{12}, \tag{3–44}$$
$$6 \times 10^{6}, 0.1, 2.4 \times 10^{11}, 7 \times 10^{5}, 0.1, 2.35 \times 10^{11}\}.$$

The adaptation gains Γ_r in (3–44) are used to enable the adaptive estimate to sufficiently change relative to the large values of the uncertain parameters in θ_r. Smaller adaptation gains could be used to obtain different results. The initial conditions for the robot coordinates and the mass-spring position were (in [m])

$$\begin{bmatrix} x_{r1}(0) & x_{r2}(0) & x_m(0) \end{bmatrix} = \begin{bmatrix} 0.008 & 0.481 & 0.202 \end{bmatrix}.$$

The initial velocity of the robot and mass-spring were zero, and the desired mass-spring position was (in [mm])

$$x_{md} = 232.$$

That is, the tip of the second link of the robot was initially 224 [mm] from the desired setpoint, and 194 [mm] from x_0 along the X_1-axis (see Fig. 2–1). Once the initial impact occurs, the robot is required to depress the spring (item (1) in Fig. 2–1) to move the mass 30 [mm] along the X_1-axis.

The mass-spring and robot errors (i.e., $e(t)$) are shown in Fig. 4–1 and Fig. 3–2. The peak steady-state position error of the end-point of the second link of the robot along the X_1-axis (i.e., $|e_{r1}(t)|$) and along the X_2-axis (i.e., $|e_{r2}(t)|$) are 0.212 [mm] and 5.77 [μm], respectively. The peak steady-state position error of the mass (i.e., $|e_m(t)|$) is 2.72 [μm]. The 0.212 [mm] maximum steady state error in $|e_{r1}(t)|$

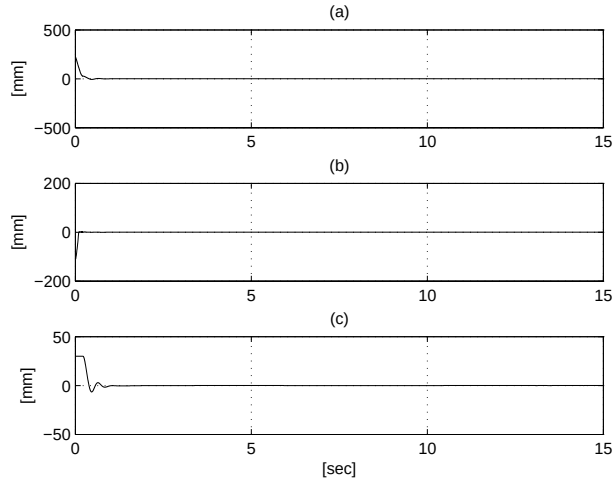

Figure 3–1: The mass-spring and robot errors $e(t)$. Plot (a) indicates the position error of the robot tip along the X_1-axis (i.e., $e_{r1}(t)$), (b) indicates the position error of the robot tip along the X_2-axis (i.e., $e_{r2}(t)$), and (c) indicates the position error of the mass-spring (i.e., $e_m(t)$).

is due to the $Y_d\hat{\theta}_{dk}(t)$ term of $x_{rd1}(t)$ in (3–11) where $Y_d(x_m)$ is approximately 0.03 [m], and $\hat{\theta}_{dk}(t)$ has a maximum steady state value of 0.007 $[\frac{N/m}{N/m}]$, yielding 0.21 [mm] error. All of the other terms in $e_{r1}(t)$ are negligible at steady state.

The input control torques in (3–22) are shown in Fig. 3–3 and Fig. 3–4. To constrain the impact force to a level that ensured the aluminum plate did not flex to the point of contact with the capacitance probe, the computed torques are artificially saturated. Fig. 3–3 depicts the computed torques, and Fig. 3–4 depicts the actual torques (solid line) along with the computed torques (dashed line). The resulting desired trajectory along the X_1-axis (i.e., $x_{rd1}(t)$) is depicted in Fig. 3–5, and the desired trajectory along the X_2-axis was chosen as $x_{rd2} = 370$ [mm]. Fig. 3–6 depicts the value of $\hat{\theta}_{dk}(t) \in \mathbb{R}$, and Fig. 3–7 - Fig. 3–9 depict the values of $\hat{\theta}_r(t) \in \mathbb{R}^{10}$. The order of the curves in the plots is based on the relative scale of the parameter estimates rather than numerical order in $\hat{\theta}_r(t)$. A video of the experiment is provided in [46].

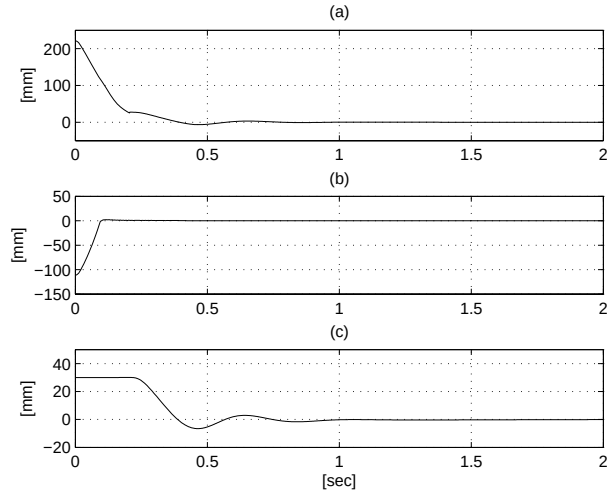

Figure 3–2: The mass-spring and robot errors $e(t)$ during the initial two seconds.

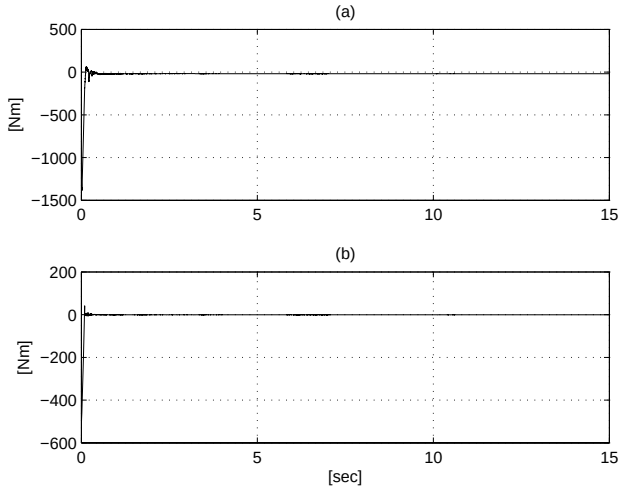

Figure 3–3: Computed control torques $J^T(q)F(t)$ for the (a) base motor and (b) second link motor.

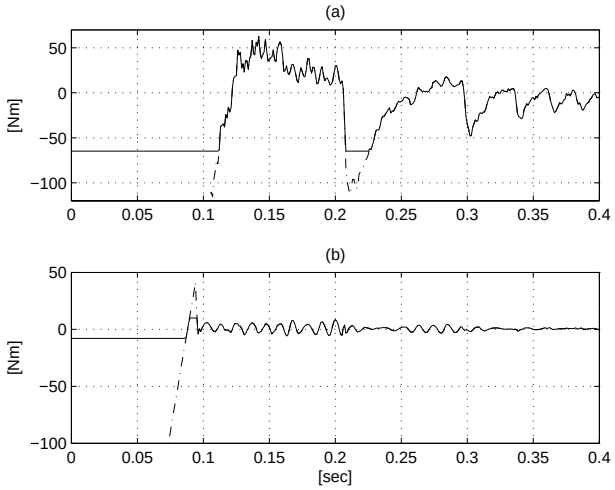

Figure 3–4: Applied control torques $J^T(q)F(t)$ (solid line) versus computed control torques (dashed line) for the (a) base motor and (b) second link motor.

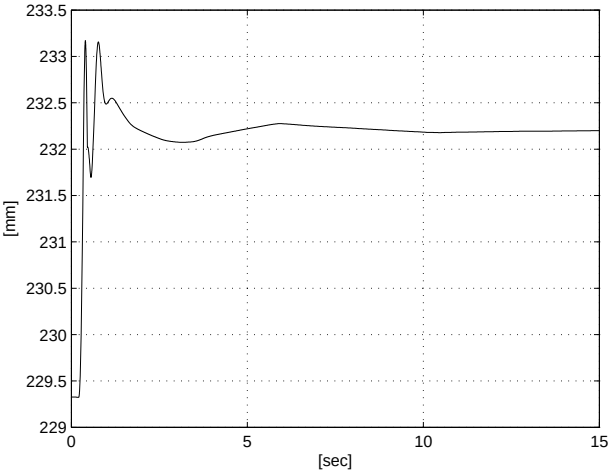

Figure 3–5: Computed desired robot trajectory, $x_{rd1}(t)$.

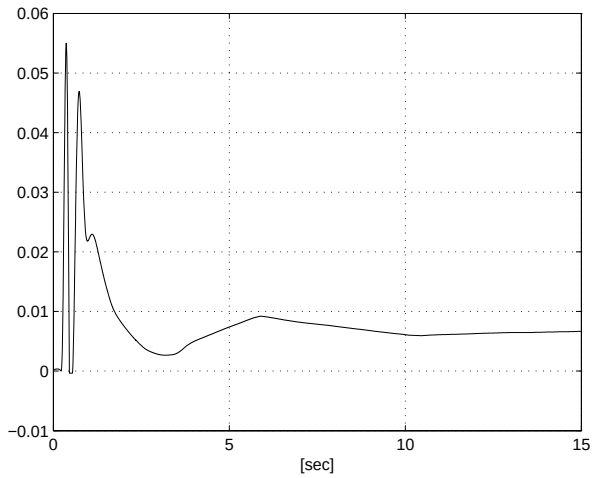

Figure 3–6: Unitless parameter estimate $\hat{\theta}_{dk}(t)$ introduced in (3–13).

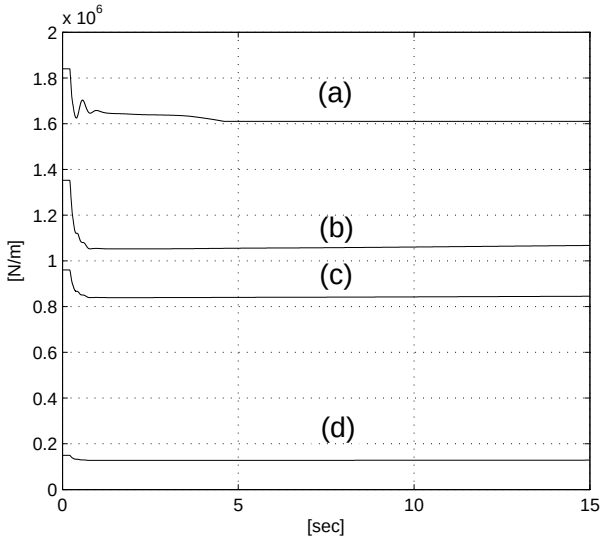

Figure 3–7: Estimate for the unknown constant parameter vector $\hat{\theta}_r(t)$. (a) $\hat{\theta}_{r10}(t) = K_I$, (b) $\hat{\theta}_{r4}(t) = \frac{K_I m_s}{m}$, (c) $\hat{\theta}_{r1}(t) = \frac{K_I m_1}{m}$, and (d) $\hat{\theta}_{r7}(t) = \frac{K_I m_2}{m}$, where m_1, $m_2 \in \mathbb{R}$ denote the mass of the first and second link of the robot, $m_s \in \mathbb{R}$ denotes the mass of the motor connected to the second link of the robot, and $m \in \mathbb{R}$ denotes the mass of the mass-spring system.

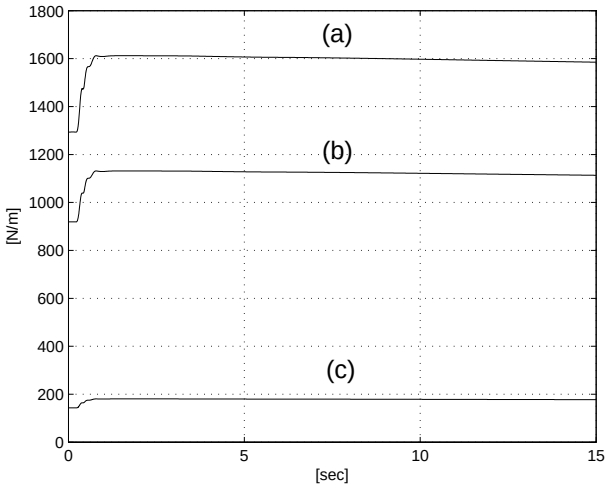

Figure 3–8: Estimate for the unknown constant parameter vector $\hat{\theta}_r(t)$. (a) $\hat{\theta}_{r5}(t) = \frac{k_s m_s}{m}$, (b) $\hat{\theta}_{r2}(t) = \frac{k_s m_1}{m}$, and (c) $\hat{\theta}_{r8}(t) = \frac{k_s m_2}{m}$.

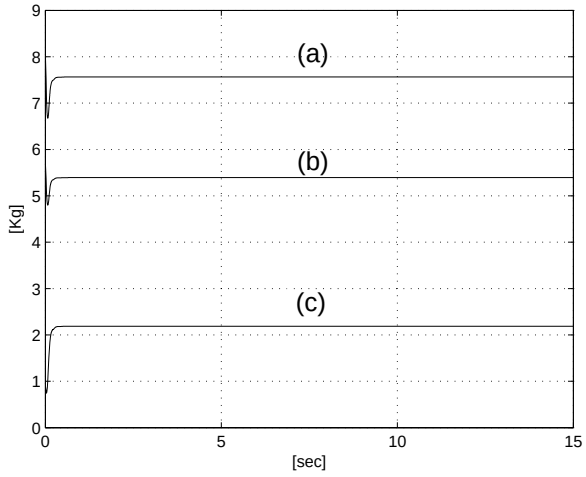

Figure 3–9: Estimate for the unknown constant parameter vector $\hat{\theta}_r(t)$. (a) $\hat{\theta}_{r6}(t) = m_s$, (b) $\hat{\theta}_{r3}(t) = m_1$, and (c) $\hat{\theta}_{r9}(t) = m_2$.

3.5 Concluding Remarks

An adaptive nonlinear Lyapunov-based controller is proven to regulate the states of a planar robot colliding with an unactuated mass-spring system. The continuous controller yields global asymptotic regulation of the spring-mass and robot links. New control design, error system development and stability analysis techniques were required to compensate for the fact that the dynamics changed from an uncoupled state to a coupled state. Experimental results are provided to illustrate the successful performance of the controller. Sufficient conditions developed in the stability analysis indicate that the control gains should be selected large enough to minimize the closed-loop steady state error, but high gains could result in large torques for large initial errors. The high gain problem is exacerbated in the developed result because of the presence of the estimated impact stiffness coefficient. The experimental results were obtained by artificially saturating the torque to prevent damage to the capacitance probe. These issues point to a need to develop controllers that account for limited actuation which we will discuss in Chapter 4.

CHAPTER 4
AN IMPACT FORCE LIMITING ADAPTIVE CONTROLLER FOR A ROBOTIC SYSTEM UNDERGOING A NON-CONTACT TO CONTACT TRANSITION

Similar to Chapter 2 and 3, the objective of this chapter is also to control a robot from a non-contact initial condition to a desired (in-contact) position so that the mass-spring system is regulated to a desired compressed state. When the controllers in Chapter 2 and Chapter 3 were implemented in the presence of large initial conditions, violent impacts between the robot and the mass-spring system resulted. In fact, the controller was artificially saturated (the saturation effects were not considered in the stability analysis) to reduce the impact forces so that the mass deflection would not destroy a capacitance probe. These results provide the motivation for the control development in this chapter. Specifically, the feedback elements for the continuous controller in Chapter 3 are contained inside of hyperbolic tangent functions as a means to limit the impact forces resulting from large initial conditions as the robot transitions from non-contact to contact states. The main challange of this work is that the use of saturated feedback does not allow some coupling terms to be canceled in the stability analysis, resulting in the need to develop state dependent upper bounds that reduce the stability to a semi-global result. New control development, closed-loop error systems, and Lyapunov-based stability analysis arguements are used to conclude the result. Experimental results are provided that successfully demonstrate the control objective.

This chapter is organized as follows. The associated properties are provided in Section 4.1. Section 4.2 describes the error system and control development

followed by the stability analysis in Section 4.3. Section 4.4 describes the experimental results that indicate the successful performance of the proposed controller followed by conclusion in Section 4.5.

4.1 Properties

Remark 4.1: To aid the subsequent control design and analysis, we define the vector $Tanh(\cdot) \in \mathbb{R}^n$ as follows

$$Tanh(\delta) \triangleq [\tanh(\delta_1), ..., \tanh(\delta_n)]^T \tag{4–1}$$

where $\delta \triangleq [\delta_1, ..., \delta_n]^T \in \mathbb{R}^n$.

Property 4.1: The following inequalities are valid for all $\xi = [\xi_1, ..., \xi_n]^T \in \mathbb{R}^n$ [1]

$$\begin{aligned} ||\xi|| \ &\geq ||Tanh(\xi)|| \\ ||\xi|| + 1 &\geq \frac{||\xi||}{\tanh(||\xi||)} \end{aligned} \tag{4–2}$$

$$||\xi||^2 \geq \sum_{i=1}^{n} \ln(\cosh(\xi_i)) \geq \ln(\cosh(||\xi||)) \tag{4–3}$$

$$\begin{aligned} \xi^T Tanh(\xi) &\geq Tanh^T(\xi) Tanh(\xi) = ||Tanh(\xi)||^2 \\ &\geq \tanh^2(||\xi||). \end{aligned} \tag{4–4}$$

4.2 Error System and Control Development

The subsequent control design is based on integrator backstepping methods. A desired trajectory is designed for the robot (i.e., a virtual control input) to ensure the robot converges to and impacts with the mass, and to ensure that the robot regulates the mass to the desired position. Since the robot trajectory can not be controlled directly, a force controller is developed to ensure that the robot tracks the desired trajectory despite the transition from free motion to an impact collision and despite uncertainties throughout the MSR system.

4.2.1 Control Objective

As in Chapter 2 and 3, the control objective is to regulate the states of the mass-sping system via a two-link planar robot that transitions from non-contact to contact with the mass-spring through an impact collision. An additional objective in this chapter is to limit the impact force to prevent damage to the robot or the environment (i.e., the mass-spring system). A regulation error, denoted by $e(t) \in \mathbb{R}^3$, is defined to quantify this objective as

$$e \triangleq \begin{bmatrix} e_m & e_r^T \end{bmatrix}^T,$$

where $e_r(t) \triangleq [e_{r1}(t), e_{r2}(t)]^T \in \mathbb{R}^2$ and $e_m(t) \in \mathbb{R}$ denote the regulation error for the end-point of the second link of the robot and mass-spring system (see Fig. 1–1), respectively, and are defined as

$$e_r \triangleq x_{rd} - x_r \qquad e_m \triangleq x_{md} - x_m. \tag{4–5}$$

In (4–5), $x_{md} \in \mathbb{R}$ denotes the constant known desired position of the mass, and $x_{rd}(t) \triangleq [x_{rd1}(t), x_{rd2}]^T \in \mathbb{R}^2$ denotes the desired position of the end-point of the second link of the robot. The subsequent development is based on the assumption that $q(t)$, $\dot{q}(t)$, $x_m(t)$, and $\dot{x}_m(t)$ are measurable, and that $x_r(t)$ and $\dot{x}_r(t)$ can be obtained from $q(t)$ and $\dot{q}(t)$. To facilitate the subsequent control design and stability analysis, filtered tracking errors, denoted by $\eta_m(t) \in \mathbb{R}$ and $r_r(t) \in \mathbb{R}^2$, are defined as [42]

$$\begin{aligned} \eta_m &\triangleq \dot{e}_m + \alpha_1 \tanh(e_m) + \alpha_2 \tanh(e_f) \\ r_r &\triangleq \dot{e}_r + \alpha e_r, \end{aligned} \tag{4–6}$$

where α, α_1, $\alpha_2 \in \mathbb{R}$ are positive, constant gains, and $e_f(t) \in \mathbb{R}$ is an auxiliary filter variable designed as [42]

$$\dot{e}_f \triangleq -\alpha_3 \tanh(e_f) + \alpha_2 \tanh(e_m) - k_1 \cosh^2(e_f)\eta_m, \tag{4–7}$$

where $k_1 \in \mathbb{R}$ is a positive constant control gain, and $\alpha_3 \in \mathbb{R}$ is a positive constant filter gain.

4.2.2 Closed-Loop Error System

In this section, the closed-loop error system for η_m is exactly the same as in (3-5)-(3-15) in Chapter 3. The open-loop robot error system can be obtained by taking the time derivative of $r_r(t)$ and premultiplying by the robot inertia matrix as

$$\bar{M}\dot{r}_r = Y_r\theta_r - \bar{C}r_r - F, \tag{4–8}$$

where (1–9), (4–5), and (4–6) were utilized, and

$$Y_r\theta_r \triangleq \bar{M}\ddot{x}_{rd} + \alpha\bar{M}\dot{e}_r + \bar{h} + \bar{C}\dot{x}_{rd} + \alpha\bar{C}x_{rd} + \begin{bmatrix} K_I\Lambda(x_{r1} - x_m) \\ 0 \end{bmatrix} - \alpha\bar{C}x_r,$$

where $Y_r(x_r, \dot{x}_r, x_m, \dot{x}_m, e_f, \eta_m, t) \in \mathbb{R}^{2\times P}$ denotes a known regression matrix, and $\theta_r \in \mathbb{R}^P$denotes an unknown constant parameter vector. By making substitutions from the dynamic model and the previous error systems, $\ddot{x}_{rd}(t)$ can be expressed without a dependance on acceleration terms. Based on (4–8) and the subsequent stability analysis, the robot force control input is designed as

$$F \triangleq Y_r\hat{\theta}_r + Tanh(e_r) + k_3 Tanh(r_r), \tag{4–9}$$

where $k_3 \in \mathbb{R}$ is a positive constant control gain, and $\hat{\theta}_r(t) \in \mathbb{R}^P$ is an estimate for θ_r generated by the following adaptive update law

$$\dot{\hat{\theta}}_r \triangleq proj(\Gamma_r Y_r^T r_r). \tag{4–10}$$

In (4–10), $\Gamma_r \in \mathbb{R}^{P\times P}$ is a positive definite, constant, diagonal, adaptation gain matrix, and $proj(\cdot)$ denotes a projection algorithm utilized to guarantee that the $i-th$ element of $\hat{\theta}_r(t)$ can be bounded as

$$\underline{\theta}_{ri} \leq \hat{\theta}_{ri} \leq \bar{\theta}_{ri}, \tag{4–11}$$

where $\underline{\theta}_{ri}$, $\bar{\theta}_{ri} \in \mathbb{R}$ denote known, constant lower and upper bounds for each element of $\theta_r(t)$, respectively.

The closed-loop error system for $r_r(t)$ can be obtained after substituting (4–9) into (4–8) as

$$\bar{M}\dot{r}_r = Y_r\tilde{\theta}_r - \bar{C}r_r - Tanh(e_r) - k_3 Tanh(r_r). \tag{4–12}$$

In (4–12), the parameter estimation error $\tilde{\theta}_r(t) \in \mathbb{R}^P$ is defined as

$$\tilde{\theta}_r \triangleq \theta_r - \hat{\theta}_r. \tag{4–13}$$

4.3 Stability Analysis

Theorem: The controller given by (3–11), (3–13), (4–9), and (4–10) ensures semi-global asymptotic regulation of the MSR system in the sense that

$$|e_m(t)| \to 0 \qquad \|e_r(t)\| \to 0 \quad as \quad t \to \infty$$

provided the following sufficient gain conditions are satisfied:

$$k_{n1} > \frac{1}{4\alpha_2 \min\left\{\alpha_1 k_2 \underline{\zeta}_K,\ \alpha_3 k_2 \underline{\zeta}_K,\ \alpha_2\right\}} \tag{4–14}$$

$$\alpha_2 > \max\left\{\frac{1}{4\alpha}, \frac{\zeta_{x_m}^2}{\lambda}\right\} \bar{\zeta}_K^2 \tag{4–15}$$

$$k_3\alpha > \left(\sqrt{\frac{2V_u}{a_1}} + 1\right)^2 \tag{4–16}$$

where $V_u \in \mathbb{R}$ is defined as

$$V_u \triangleq \max\left\{\lambda_1 \left\|\bar{z}(0)\right\|^2 + \zeta_\theta,\, 5\lambda_1(\tanh^{-1}(\sqrt{\frac{\varepsilon_x}{\lambda}}))^2 + \zeta_\theta\right\},$$

$\lambda \in \mathbb{R}$ is a known positive constant, and a_1, α, α_1, α_2, α_3, k_{n1}, k_2, k_3, λ_1, ζ_{x_m}, ζ_{x_r}, $\underline{\zeta}_K$, and $\overline{\zeta}_K$ are defined in (1–4), (1–11), (3–1), (3–11), (3–12), (4–6), (4–7), and (4–9).

As in the previous chapters, the subsequent analysis is separated into two cases: contact and non-contact. For the non-contact case, the stability analysis indicates the controller and error signals are bounded and converge to an arbitrarily small region where contact must occur. When contact occurs, a Lyapunov analysis is provided that illustrates the MSR system asymptotically converges to the desired setpoint.

Proof: Let $V(t) \in \mathbb{R}$ denote the following non-negative, radially unbounded function (i.e. a Lyapunov function candidate):

$$V \triangleq \frac{1}{2}r_r^T\bar{M}r_r + \frac{1}{2}\tilde{\theta}_r^T\Gamma_r^{-1}\tilde{\theta}_r + \frac{1}{2}\tilde{\theta}_{dk}^T K_I\Gamma^{-1}\tilde{\theta}_{dk} + e_r^T e_r + \frac{1}{2}m\eta_m^2 \tag{4–17}$$
$$+ k_2K_I\left[\ln\left(\cosh(e_m)\right) + \ln\left(\cosh\left(e_f\right)\right)\right] + \ln(\cosh(e_{r1})) + \ln(\cosh(e_{r2}))$$

where (1–11) and (4–3) can be utilized to bound $V(t)$ as

$$\frac{a_1}{2}||r_r||^2 \leq V \leq \lambda_1\left\|\bar{z}\right\|^2 + \zeta_\theta \tag{4–18}$$

where $\lambda_1, \zeta_\theta \in \mathbb{R}$ and $\bar{z} \in \mathbb{R}^7$ are defined as

$$\begin{aligned}\lambda_1 &\triangleq \max\{\frac{a_2}{2}, 3, \frac{m_u}{2}, k_2\overline{\zeta}_K\}\\ \zeta_\theta &\triangleq \frac{1}{2}\overline{\zeta}_K\zeta_{\theta_{dk}}^2\Gamma^{-1} + \frac{1}{2}\lambda_{\max}\{\Gamma_r^{-1}\}\left\|\zeta_{\theta_r}\right\|^2\\ \bar{z} &\triangleq [r_r^T, e_r^T, \eta_m, e_m, e_f]^T\end{aligned} \tag{4–19}$$

where $\lambda_{\max}\{\cdot\} \in \mathbb{R}$ denotes the maximum eigenvalue of a matrix, and $\zeta_{\theta_{dk}}$,$\|\zeta_{\theta_r}\|$ are the known upper bounds of $\tilde{\theta}_{dk}(t)$ and $\left\|\tilde{\theta}_r(t)\right\|$, respectively. After using (1–12),

(3–12), (3–13), (3–15), (4–4), (4–6), (4–7), (4–10), and (4–12), the time derivative of (4–17) can be determined as

$$\begin{aligned}\dot{V} \leq & -k_3 \tanh^2(\|r_r\|) - \alpha_1 k_2 K_I \tanh^2(e_m) - \alpha_3 k_2 K_I \tanh^2(e_f) \\ & + 2e_r^T r_r - 2\alpha e_r^T e_r - 3\alpha_2 \eta_m^2 - k_{n1}\zeta_1^2 \alpha_2 \eta_m^2 - \alpha \tanh^2(\|e_r\|) \\ & + \eta_m \left[K_I \left(x_{rd1} - \Lambda x_{r1}\right) + K_I \left(\Lambda x_m - x_m\right) + \chi\right].\end{aligned} \tag{4–20}$$

The expression in (4–20) will now be examined under two different scenarios.

Case 1-Non-contact: For this case, the systems are not in contact ($\Lambda = 0$) and (4–20) can be rewritten as

$$\begin{aligned}\dot{V} \leq & -k_3 \tanh^2(\|r_r\|) - \alpha_1 k_2 K_I \tanh^2(e_m) - \alpha_3 k_2 K_I \tanh^2(e_f) \\ & + 2e_r^T r_r - 2\alpha e_r^T e_r - 3\alpha_2 \eta_m^2 - k_{n1}\zeta_1^2 \alpha_2 \eta_m^2 - \alpha \tanh^2(\|e_r\|) \\ & + \eta_m \left[K_I x_{rd1} - K_I x_m + \chi\right].\end{aligned} \tag{4–21}$$

Based on (3–1), (3–9), and (4–5), the expression in (4–21) can be rewritten as

$$\begin{aligned}\dot{V} \leq & -k_3 \tanh^2(\|r_r\|) - \alpha_1 k_2 \underline{\zeta}_K \tanh^2(e_m) - \alpha_3 k_2 \underline{\zeta}_K \tanh^2(e_f) \\ & - 2\alpha_2 \eta_m^2 - \alpha \tanh^2(\|e_r\|) \\ & - \left[\alpha \|e_r\|^2 - \overline{\zeta}_K |\eta_m| \|e_r\|\right] - \left[k_{n1}\zeta_1^2 \alpha_2 \eta_m^2 - \zeta_1 \|z\| |\eta_m|\right] \\ & - \left[\alpha_2 \eta_m^2 - \overline{\zeta}_K |\eta_m| |x_m - x_{r1}|\right] - [\alpha \|e_r\|^2 - 2\|e_r\| \|r_r\|].\end{aligned} \tag{4–22}$$

After completing the square in the bracketed terms, (4–22) can be expressed as

$$\begin{aligned}\dot{V} \leq & -\beta \|z\|^2 - \alpha \tanh^2(\|e_r\|) - \left(\alpha_2 - \frac{\overline{\zeta}_K^2}{4\alpha}\right) \eta_m^2 \\ & + \frac{\overline{\zeta}_K^2 (x_m - x_{r1})^2}{4\alpha_2} - \left(k_3 - \frac{\|r_r\|^2}{\alpha \tanh^2(\|r_r\|)}\right) \tanh^2(\|r_r\|)\end{aligned} \tag{4–23}$$

where $\beta \in \mathbb{R}$ is defined as

$$\beta = \min\left\{\alpha_1 k_2 \underline{\zeta}_K,\ \alpha_3 k_2 \underline{\zeta}_K,\ \alpha_2\right\} - \frac{1}{4\alpha_2 k_{n1}} > 0$$

provided k_{n1} is selected according to (4–14). Provided α_2 is selected according to the sufficient condition in (4–15), then (1–4), (4–2), (4–18), and the fact that

$$\zeta_{x_r} \leq x_{r1} < x_m \leq \zeta_{x_m} \tag{4–24}$$

for the non-contact case, can be used to rewrite (4–23) as

$$\begin{aligned} \dot{V} \leq & -\beta \left\| z \right\|^2 - \alpha \tanh^2(\left\| e_r \right\|) + \varepsilon_x \\ & - \left(k_3 - \frac{1}{\alpha} \left(\sqrt{\frac{2V}{a_1}} + 1 \right)^2 \right) \tanh^2(\left\| r_r \right\|). \end{aligned} \tag{4–25}$$

In (4–25), $\varepsilon_x \in \mathbb{R}$ is a known positive arbitrarily small constant that is defined as

$$\varepsilon_x \triangleq \frac{\overline{\zeta}_K^2 \zeta_{x_m}^2}{\alpha_2}.$$

Provided the following sufficient condition is satisfied

$$k_3 \alpha > \left(\sqrt{\frac{2V}{a_1}} + 1 \right)^2, \tag{4–26}$$

the expression in (4–25) can be expressed as

$$\dot{V} \leq -\lambda \left\| y \right\|^2 + \varepsilon_x \tag{4–27}$$

where λ is a known constant and $y \in \mathbb{R}^5$ is defined as

$$y \triangleq \begin{bmatrix} z^T & \tanh(\left\| e_r \right\|) & \tanh(\left\| r_r \right\|) \end{bmatrix}^T. \tag{4–28}$$

In (4–27), ε_x can be made arbitrarily small by making α_2 large. Based on (4–17) and (4–27), if $\lambda \left\| y(t) \right\|^2 > \varepsilon_x$, then Barbalat's Lemma can be used to conclude that $\dot{V}(t) \to 0$ since $V(t)$ is lower bounded, $\dot{V}(t)$ is negative semi-definite, and $\dot{V}(t)$ can be shown to be uniformly continuous. As $\dot{V}(t) \to 0$, eventually $\lambda \left\| y(t) \right\|^2 \leq \varepsilon_x$. While $\lambda \left\| y(t) \right\|^2 > \varepsilon_x$, (4–17), (4–18), and (4–27) can be used to conclude that

$V(t) \in \mathcal{L}_\infty$, and the sufficient condition given in (4–26) can be expressed as

$$k_3\alpha > \left(\sqrt{\frac{2\left(\lambda_1 \left\|\bar{z}(0)\right\|^2 + \zeta_\theta\right)}{a_1}} + 1 \right)^2. \tag{4–29}$$

Provided $\alpha_2 > \frac{\overline{\zeta}_K^2 \zeta_{xm}^2}{\lambda}$ then eventually $\lambda \left\|y(t)\right\|^2 \leq \varepsilon_x < \lambda$. Based on (3–10) and (4–28), the fact that $\lambda \left\|y(t)\right\|^2 \leq \varepsilon_x < \lambda$ can be used to conclude that $e_m(t)$, $e_f(t)$, $e_r(t)$, $r_r(t)$, $\eta_m(t) \in \mathcal{L}_\infty$. Since $\tilde{\theta}_r(t)$ and $\tilde{\theta}_{dk}(t) \in \mathcal{L}_\infty$ from the use of a projection algorithm, the previous facts can be used to conclude that $V(t) \in \mathcal{L}_\infty$. Signal chasing arguments can be used to prove the remaining closed-loop signals are also bounded during the non-contact case provided (4–26) is satisfied.

If the initial conditions for $V(0)$ are large enough that $\lambda \left\|y(t)\right\|^2 > \varepsilon_x$, then the condition in (4–29) is sufficient. However, if the initial conditions for $V(0)$ are inside the region defined by ε_x, then $V(t)$ can grow larger until $\lambda \left\|y(t)\right\|^2 \leq \varepsilon_x$. Therefore, further development is required to determine how large $V(t)$ can grow so that the sufficient condition in (4–26) can be satisfied. When $V(0)$ is inside the region defined by ε_x, then

$$\left\|y(t)\right\| \leq \sqrt{\frac{\varepsilon_x}{\lambda}}. \tag{4–30}$$

The expression in (4–30) can be used along with (3–10), (4–19), and (4–28) to conclude that

$$\left\|\bar{z}(t)\right\| \leq \sqrt{5} \tanh^{-1}\left(\sqrt{\frac{\varepsilon_x}{\lambda}}\right). \tag{4–31}$$

The inequality in (4–31) can be used along with (4–18) and (4–19) to rewrite the sufficient condition in (4–26) as

$$k_3\alpha > \left(\sqrt{\frac{2\left(5\lambda_1 (\tanh^{-1}(\sqrt{\frac{\varepsilon_x}{\lambda}}))^2 + \zeta_\theta\right)}{a_1}} + 1 \right)^2. \tag{4–32}$$

Hence, the final sufficient condition for (4–26) is given by (4–16). That is, provided k_{n1}, α, α_2, and k_3 are selected larger than known constants (that depends on the

initial conditions of the states) according to (4–14)-(4–16) then the all the states converge to an arbitrarily small neighborhood. Development has been provided (see Section 3.3) to prove that contact with the mass-spring system is ensured within this neighborhood.

Case 2-Contact: For the case when the dynamic systems collide ($\Lambda = 1$) and the two dynamic systems become coupled[1] , then (4–20) can be rewritten as

$$\begin{aligned}\dot{V} \leq & -k_3 \tanh^2(\|r_r\|) - \alpha_1 k_2 \underline{\zeta}_K \tanh^2(e_m) - \alpha_3 k_2 \underline{\zeta}_K \tanh^2(e_f) \\ & - 3\alpha_2 \eta_m^2 - \alpha \tanh^2(\|e_r\|) - \left[\alpha \|e_r\|^2 - \overline{\zeta}_K |\eta_m| \|e_r\|\right] \\ & - \left[k_{n1}\zeta_1^2 \alpha_2 \eta_m^2 - \zeta_1 \|z\| |\eta_m|\right] - \left[\alpha \|e_r\|^2 - 2 \|e_r\| \|r_r\|\right],\end{aligned}$$

where (3–1) was substituted for K_I and (3–9) was substituted for $\chi(e_m, e_f, \eta_m, t)$. Completing the square on the three bracketed terms yields

$$\begin{aligned}\dot{V} \leq & -\beta \|z\|^2 - \alpha \tanh^2(\|e_r\|) - \left(\alpha_2 - \frac{\overline{\zeta}_K^2}{4\alpha}\right) \eta_m^2 \\ & - \left(k_3 - \frac{\|r_r\|^2}{\alpha \tanh^2(\|r_r\|)}\right) \tanh^2(\|r_r\|).\end{aligned} \tag{4–33}$$

Because (4–17) is non-negative, as long as (4–14)-(4–16) are satisfied, (4–33) is negative semi-definite, and $r_r(t)$, $\tilde{\theta}_r(t)$, $\tilde{\theta}_{dk}(t)$, $e_r(t)$, $e_m(t)$, $e_f(t)$, and $\eta_m(t) \in \mathcal{L}_\infty$. Due to the fact that $e_m(t)$, $e_f(t)$, and $\eta_m(t) \in \mathcal{L}_\infty$, the expression in (4–6) can be used to conclude that $\dot{e}_m(t) \in \mathcal{L}_\infty$ (and hence, $e_m(t)$ is uniformly continuous (UC)). Due to the fact that $\dot{e}_m(t) \in \mathcal{L}_\infty$, $\dot{x}_m(t) \in \mathcal{L}_\infty$. Based on (1–4), $x_m(t) \in \mathcal{L}_\infty$. Previous facts can be used to prove that $x_{rd}(t) \in \mathcal{L}_\infty$, and since $e_r(t) \in \mathcal{L}_\infty$, then $x_r(t) \in \mathcal{L}_\infty$. Due to the fact that $e_f(t)$, $e_m(t)$, $\eta_m(t) \in \mathcal{L}_\infty$, (4–7) can be used to conclude that $\dot{e}_f(t) \in \mathcal{L}_\infty$. The expression in (3–5) can then be used to conclude

[1] The dynamic systems can separate after impact, however this case can still be analyzed under the Non-Impact section of the stability analysis.

that $\dot{\eta}_m(t) \in \mathcal{L}_\infty$ (and hence, $\eta_m(t)$ is UC). Based on (4–6) and the fact that $r_r(t)$ and $e_r(t) \in \mathcal{L}_\infty$, $\dot{e}_r(t) \in \mathcal{L}_\infty$. Also, based on (3–14) and the fact that $x_m(t)$, $e_m(t)$, $e_f(t)$, $\eta_m(t)$, and $\dot{x}_m(t) \in \mathcal{L}_\infty$, the expression in (3–11) can be used to prove that $\dot{x}_{rd}(t) \in \mathcal{L}_\infty$. Based on the fact that $\dot{e}_r(t)$ and $\dot{x}_{rd}(t) \in \mathcal{L}_\infty$, the expression in (4–5) can be used to prove that $\dot{x}_r(t) \in \mathcal{L}_\infty$. Given that $x_r(t)$, $\dot{x}_r(t)$, $x_m(t)$, $\dot{x}_m(t)$, $e_f(t)$, and $\eta_m(t) \in \mathcal{L}_\infty$, $Y_r(\cdot) \in \mathcal{L}_\infty$. The expression in (4–9), (4–11) can then be used to prove that $F(t) \in \mathcal{L}_\infty$. The expression in (4–12) can be used to conclude that $\dot{r}_r(t) \in \mathcal{L}_\infty$ (and hence, $r_r(t)$ is UC). Since $e_m(t)$ and $r_r(t)$ are UC which implies $\tanh(e_m(t))$ and $\tanh(\|r_r(t)\|)$ are also UC, and the fact that $\tanh(e_m(t))$, $\tanh(\|r_r(t)\|)$, and $\eta_m(t)$ are square integrable, Barbalat's Lemma can be used to conclude that $\tanh(e_m(t))$, $\tanh(\|r_r(t)\|)$, $|\eta_m(t)| \to 0$ as $t \to \infty$, which also implies $|e_m(t)|$, $\|r_r(t)\| \to 0$ as $t \to \infty$. Based on the fact that $\|r_r(t)\| \to 0$ as $t \to \infty$, standard linear analysis methods (see Lemma A.15 of [41]) can then be used to prove that $\|e_r(t)\| \to 0 \quad \text{as} \quad t \to \infty$.

4.4 Experimental Results

With the testbed in Section 2.3, the control gains α and k_3, defined as scalars in (4–6) and (4–9), were implemented (with nonconsequential implications to the stability result) as diagonal gain matrices to provide more flexibility in the experiment. Specifically, the control gains were selected as

$$k_1 = 0.28 \quad k_2 = 0.855 \quad k_3 = diag\{110, 10\}$$
$$\alpha_1 = 60 \quad \alpha_2 = 2.8 \quad \alpha_3 = 0.06 \quad \alpha = diag\{40, 8\}.$$

The adaptation gains were selected as

$$\Gamma = 0.06$$

$$\Gamma_r = diag\{1.8 \times 10^{11}, 1.5 \times 10^{5}, 0.2, 7 \times 10^{10},$$
$$7 \times 10^{4}, 0.1, 1 \times 10^{10}, 1 \times 10^{4}, 0.01, 2.8 \times 10^{9}\}.$$

The initial conditions for the robot coordinates and the mass-spring position were (in [m])

$$\begin{bmatrix} x_{r1}(0) & x_{r2}(0) & x_m(0) \end{bmatrix} = \begin{bmatrix} 0.070 & 0.285 & 0.206 \end{bmatrix}.$$

The initial velocity of the robot and mass-spring were zero, and the desired mass-spring position was (in [mm])

$$x_{md} = 236.$$

That is, the tip of the second link of the robot was initially 166 mm from the desired setpoint and 136 mm from the initial impact point along the X_1-axis (see Fig. 2–1). Therefore, once the initial impact occurs, the robot is required to depress the spring (item (1) in Fig. 2–1) to move the mass 30 mm along the X_1-axis.

The mass-spring and robot errors (i.e., $e(t)$) are shown in Fig. 4–1. The peak steady-state position error of the robot tip along the X_1-axis (i.e., $|e_{r1}(t)|$) and along the X_2-axis (i.e., $|e_{r2}(t)|$) are 0.855 mm and 0.179 mm, respectively. The peak steady-state position error of the mass-spring (i.e., $|e_m(t)|$) is 0.184 mm.

The input control torques (i.e., $J^T(q)F(t)$) are shown in Fig. 4–2 and Fig. 4–3. The resulting desired trajectory along the X_1-axis (i.e., $x_{rd1}(t)$) is depicted in Fig. 4–4, and the desired trajectory along the X_2-axis was chosen as $x_{rd2} = 357.5$ mm. Fig. 4–5 depicts the value of $\hat{\theta}_{dk}(t) \in \mathbb{R}$ and Fig. 4–6 - Fig. 4–8 depict the values of $\hat{\theta}_r(t) \in \mathbb{R}^{10}$. The order of the curves in the plots comes from their scales rather than their numerical order in $\hat{\theta}_r(t)$.

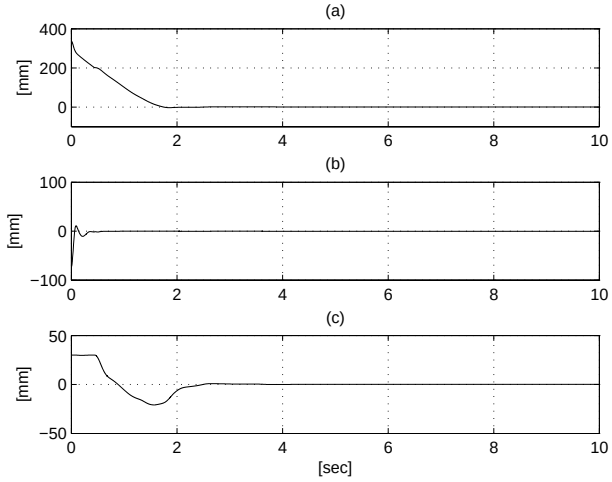

Figure 4–1: The mass-spring and robot errors $e(t)$. Plot (a) indicates the position error of the robot tip along the X_1-axis (i.e., $e_{r1}(t)$), (b) indicates the position error of the robot tip along the X_2-axis (i.e., $e_{r2}(t)$), and (c) indicates the position error of the mass-spring (i.e., $e_m(t)$).

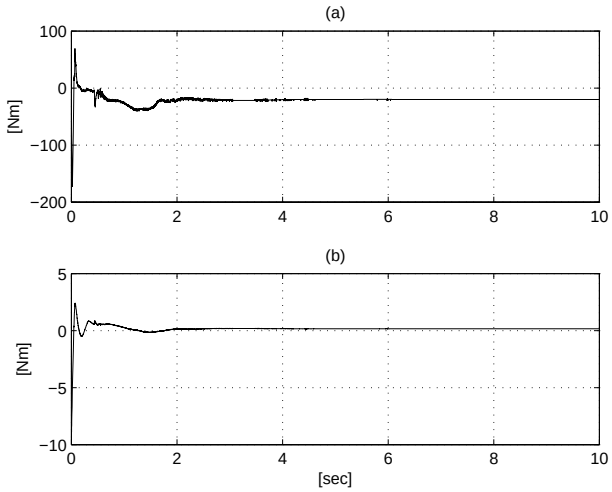

Figure 4–2: Applied control torques $J^T(q)F(t)$ for the (a) base motor and (b) second link motor.

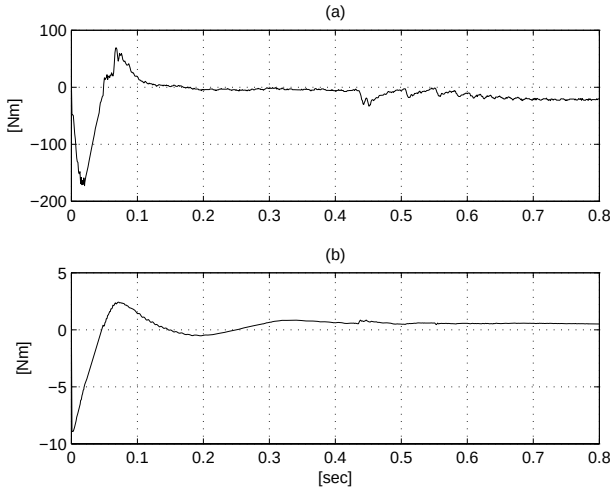

Figure 4–3: Applied control torques $J^T(q)F(t)$ for the (a) base motor and (b) second link motor during the first 0.8 second.

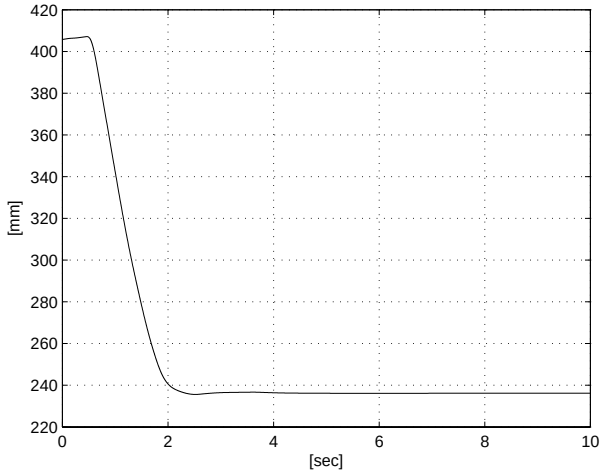

Figure 4–4: Computed desired robot trajectory, $x_{rd1}(t)$.

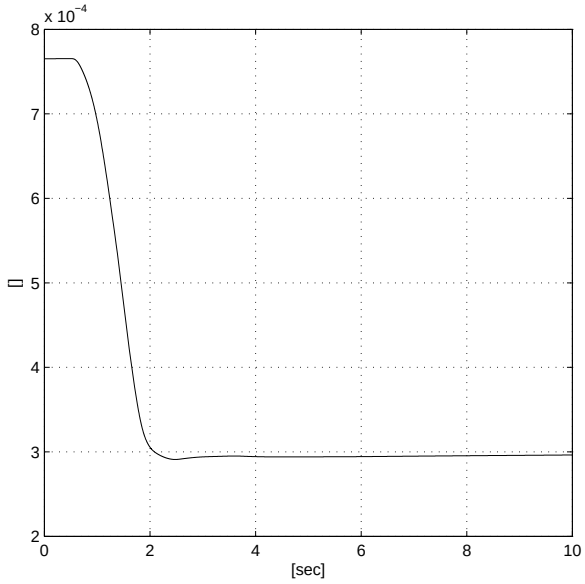

Figure 4–5: Parameter estimate $\hat{\theta}_{dk}(t)$ introduced in (3–13).

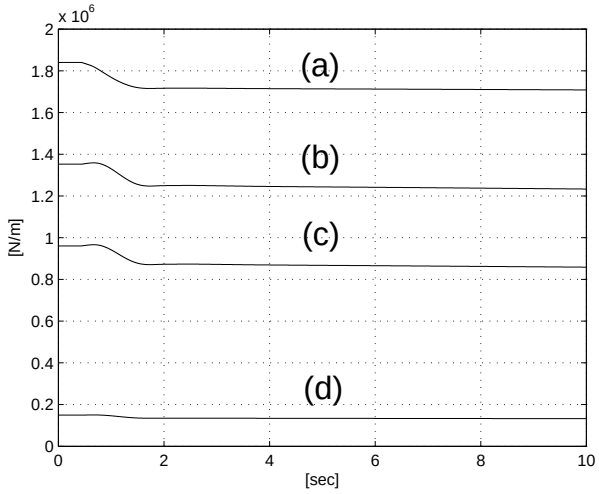

Figure 4–6: Estimate for the unknown constant parameter vector $\hat{\theta}_r(t)$. (a) $\hat{\theta}_{r10}(t) = K_I$, (b) $\hat{\theta}_{r4}(t) = \frac{K_I m_s}{m}$, (c) $\hat{\theta}_{r1}(t) = \frac{K_I m_1}{m}$, and (d) $\hat{\theta}_{r7}(t) = \frac{K_I m_2}{m}$, where m_1, $m_2 \in \mathbb{R}$ denote the mass of the first and second link of the robot, $m_s \in \mathbb{R}$ denotes the mass of the motor connected to the second link of the robot, and $m \in \mathbb{R}$ denotes the mass of the mass-spring system.

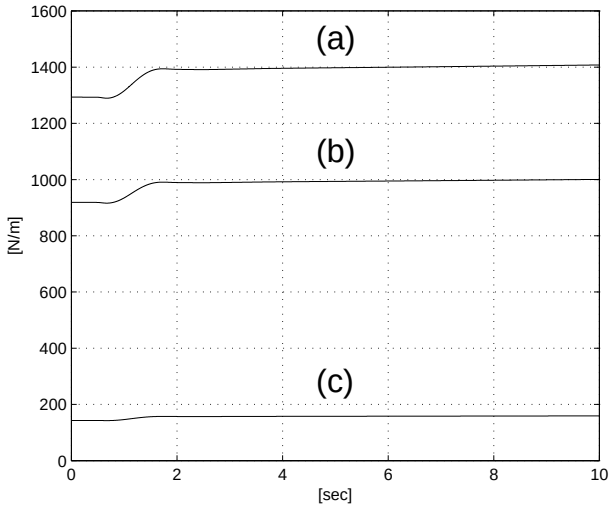

Figure 4–7: Estimate for the unknown constant parameter vector $\hat{\theta}_r(t)$. (a) $\hat{\theta}_{r5}(t) = \frac{k_s m_s}{m}$, (b) $\hat{\theta}_{r2}(t) = \frac{k_s m_1}{m}$, and (c) $\hat{\theta}_{r8}(t) = \frac{k_s m_2}{m}$.

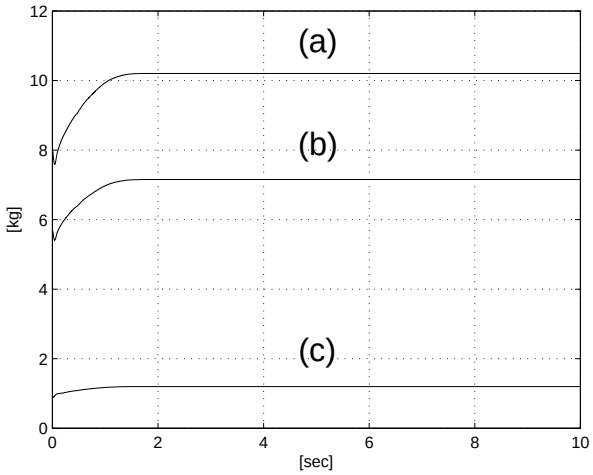

Figure 4–8: Estimate for the unknown constant parameter vector $\hat{\theta}_r(t)$. (a) $\hat{\theta}_{r6}(t) = m_s$, (b) $\hat{\theta}_{r3}(t) = m_1$, and (c) $\hat{\theta}_{r9}(t) = m_2$.

4.5 Concluding Remarks

In this chapter, we consider a two link planar robotic arm that transitions from free motion to contact with an unactuated mass-spring system. An adaptive nonlinear Lyapunov-based controller with bounded torque input amplitudes is proven to regulate the states of the system. The feedback elements for the controller in this chapter are contained inside of hyperbolic tangent functions as a means to limit the impact forces resulting from large initial conditions as the robot transitions from non-contact to contact. The continuous controller yields semi-global asymptotic regulation of the spring-mass and robot links. Experimental results are provided to illustrate the successful performance of the controller.

CHAPTER 5
CONCLUSION AND RECOMMENDATIONS

Motivated by the fact that impacts between the robot and the static environment cannot represent all the impact system applications, and discontinuous controllers require infinite control frequency (i.e., exhibit chattering) or yield degraded stability results (i.e., uniformly ultimately bounded), continuous Lyapunov-based controllers for a fully actuated dynamic systems undergoing an impact collision with another unactuated dynamic system are developed. Lyapunov-based methods are used to prove the asymptotic regulations of the mass and robot links. Unlike some other results in literature, the continuous force controller does not depend on measuring the impact force or the measurement of other acceleration terms: only the position and velocity terms of the spring-mass system and the joint angles and the angular velocities terms of the planar robotic arm are needed for the proposed controller.

Chapter 2 provides a first step at controlling the proposed impact system. The control development in Chapter 2 is based on the assumption of exact model knowledge of the system dynamics. The controller is proven to regulate the states of the system and yields global asymptotic result. In Chapter 3, the dynamic model for the system is assumed to have uncertain parameters. The control objective is defined as the desire to both regulate the system to a desired compressed state and compensate for the constant, unknown system parameters. Two linear parameterizations are designed to adapt for the unknown robot and mass-spring parameters. The controller is proven to yield global asymptotic regulation result. An extension of the developed regulation controller of Chapter 3 is presented in Chapter 4 where the feedback elements for the controller in this chpater are

contained inside of hyperbolic tanget functions as a means to limit the impact forces resulting from large initial conditions as the robot transitions from non-contact to contact states. The controller yields semi-global asymptotic regulation of the system. Experimental results are provided to illustrate the successful performance of the controller in each chapter.

Future efforts can focus on utilizing non-model based control methods such as neural networks, fuzzy logic, or robust control methods to compensate the more complex uncertainties of the system. The developed model can also be modified to control the impact between an actuated dynamic system and an unactuated dynamic system with nonlinear flexibilities. Future work could also focus on the specific application of the developed methods for applications such as docking space vehicles, walking robots, etc. Efforts could also focus on obtaining a global result of the feedback saturated case in Chapter 4.

APPENDIX A
THE EXPRESSION OF $\ddot{x}_{rd1}$ IN SECTION 2.1

Due to the fact that taking the time derivative of any expression with Λ except for $K\Lambda(x_{r1} - x_m)$ is undefined, some care has to be taken in taking the time derivative of $x_{rd1}(t)$. This is done by first taking the time derivative of (2-6) and utilizing (2-3) and (2-7), to obtain the following expression:

$$\begin{aligned}\dot{x}_{rd1} = &\frac{\alpha}{K}\left[(1-\Lambda)\left(k(x_m - x_0) + \alpha m\dot{e}_m\right)\right] + \frac{\alpha}{K}\Lambda\left[Ke_{r1} - (k_1+k_2)\, r_m\right] \\ &- \frac{\alpha^2 m}{K}(r_m - \alpha e_m) + \left(\frac{k}{K} + 1\right)\dot{x}_m + \frac{1}{mK}\,(k_1+k_2)\,(1-\Lambda)\,k(x_m - x_0) \\ &+ \frac{1}{mK}\,(k_1+k_2)\,(1-\Lambda)\,\alpha m\dot{e}_m + \frac{1}{mK}\,(k_1+k_2)\,\Lambda\left[Ke_{r1} - (k_1+k_2)\, r_m\right].\end{aligned} \tag{A–1}$$

In order to derive $\ddot{x}_{rd1}(t)$, the second time derivative of (2-6) is taken rather than the first time derivative of (A–1) to obtain

$$\ddot{x}_{rd1} = \frac{1}{K}(\alpha m\dddot{e}_m + k\ddot{x}_m + (k_1+k_2)\ddot{r}_m) + \ddot{x}_m. \tag{A–2}$$

The expression for $\dot{e}_m(t)$ can be obtained by rewriting (2-3) as

$$\dot{e}_m = r_m - \alpha e_m. \tag{A–3}$$

Differentiating (A–3) yields the following expressions for $\ddot{e}_m(t)$ and $\dddot{e}_m(t)$:

$$\ddot{e}_m = \dot{r}_m - \alpha\dot{e}_m \tag{A–4}$$

$$\dddot{e}_m = \ddot{r}_m - \alpha\ddot{e}_m. \tag{A–5}$$

By using (2-7), the expression for $\dot{r}_m(t)$ can be written as

$$\dot{r}_m = \frac{1}{m}\left[(1-\Lambda)\left(k(x_m - x_0) + \alpha m\dot{e}_m\right)\right] + \frac{1}{m}\left[K\Lambda e_{r1} - \Lambda(k_1+k_2)r_m\right]. \tag{A–6}$$

The time derivative of (2-4) is given by

$$\ddot{r}_m = \frac{1}{m}(k\dot{x}_m - K\Lambda(\dot{x}_{r1} - \dot{x}_m) + \alpha m\ddot{e}_m). \tag{A–7}$$

The dynamics for the mass-spring system $\ddot{x}_m(t)$ can be written as

$$\ddot{x}_m = \frac{1}{m}(K\Lambda(x_{r1} - x_m) - k(x_m - x_0)). \tag{A–8}$$

By using (A–2) and (A–5), the following expression can be obtained:

$$\ddot{x}_{rd1} = \frac{\alpha m}{K}(\ddot{r}_m - \alpha\ddot{e}_m) + (\frac{k}{K} + 1)\ddot{x}_m + \frac{(k_1 + k_2)}{K}\ddot{r}_m. \tag{A–9}$$

Substituting (A–4) and (A–7)-(A–9) yields

$$\begin{aligned}\ddot{x}_{rd1} = {} & \frac{\alpha}{K}\left(k\dot{x}_m - K\Lambda\left(\dot{x}_{r1} - \dot{x}_m\right) + \alpha m\ddot{e}_m\right) - \frac{\alpha^2 m}{K}\dot{r}_m + \frac{\alpha^3 m}{K}\dot{e}_m \\ & + (\frac{k}{K} + 1)\frac{1}{m}(K\Lambda\left(x_{r1} - x_m\right) - k(x_m - x_0)) \\ & + \frac{(k_1 + k_2)}{Km}\left[k\dot{x}_m - K\Lambda\left(\dot{x}_{r1} - \dot{x}_m\right) + \alpha m\ddot{e}_m\right].\end{aligned} \tag{A–10}$$

After using (A–4) and (A–6), a simplified expression for $\ddot{x}_{rd1}(t)$ can be obtained as follows:

$$\begin{aligned}\ddot{x}_{rd1} = {} & \frac{\alpha}{K}\left(k\dot{x}_m - K\Lambda\left(\dot{x}_{r1} - \dot{x}_m\right)\right) \\ & + (\frac{k}{K} + 1)\frac{1}{m}(K\Lambda(x_{r1} - x_m) - k(x_m - x_0)) \\ & + \frac{(k_1 + k_2)}{Km}\left[k\dot{x}_m - K\Lambda\left(\dot{x}_{r1} - \dot{x}_m\right)\right] \\ & + \frac{(k_1 + k_2)\,\alpha}{Km}\left(1 - \Lambda\right)\left(k(x_m - x_0)\right) \\ & + \frac{(k_1 + k_2)\,\alpha}{m}\Lambda e_{r1} - \frac{\alpha}{Km}\Lambda(k_1 + k_2)^2 r_m.\end{aligned} \tag{A–11}$$

APPENDIX B
THE EXPRESSION OF $\ddot{x}_{rd1}$ IN SECTION 3.2

Since x_{rd2} is a constant, the subsequent development is only focused on determining $\ddot{x}_{rd1}(t)$. After using (3-2), (3-4), (3-11), and (3-13), the first time derivative of $x_{rd1}(t)$ can be determined as

$$\dot{x}_{rd1} = Y_d \left(proj\left(\Gamma Y_d \eta_m\right)\right) + \left(\hat{\theta}_{dk} + 1 - k_2 \cosh^{-2}(e_m)\right) \dot{x}_m \tag{B–1}$$
$$- k_1 k_2 \left(\sinh^2(e_f) + \cosh^2(e_f)\right) \left(-\alpha_3 \tanh(e_f) + \alpha_2 \tanh(e_m) - k_1 \cosh^2(e_f)\eta_m\right).$$

Based on the fact that the projection algorithm for $\dot{\hat{\theta}}_{dk}(t)$ is designed to be sufficiently smooth [43], the expressions in (3-13) and (B–1) can be used to determine the second time derivative of $x_{rd1}(t)$ as

$$\ddot{x}_{rd1} = Y_d \frac{\partial \left(proj(\Gamma Y_d \eta_m)\right)}{\partial \eta_m} \dot{\eta}_m + \left(Y_d \frac{\partial \left(proj(\Gamma Y_d \eta_m)\right)}{\partial x_m} + 2proj\left(\Gamma Y_d \eta_m\right)\right) \dot{x}_m \tag{B–2}$$
$$- 2k_2 \cosh^{-3}(e_m) \sinh(e_m) \dot{x}_m^2 + \left(\hat{\theta}_{dk} + 1 - k_2 \cosh^{-2}(e_m)\right) \ddot{x}_m$$
$$- 4k_1 k_2 \left(\sinh(e_f) \cosh(e_f)\right) \dot{e}_f^2$$
$$- k_1 k_2 \left(\sinh^2(e_f) + \cosh^2(e_f)\right) \left(-\alpha_3 \cosh^{-2}(e_f) - 2k_1 \cosh(e_f) \sinh(e_f) \eta_m\right) \dot{e}_f$$
$$+ k_1 k_2 \left(\sinh^2(e_f) + \cosh^2(e_f)\right) \left(-\alpha_2 \cosh^{-2}(e_m) \dot{e}_m + k_1 \cosh^2(e_f) \dot{\eta}_m\right).$$

After substituting (3-4) and (3-5) into (B–2) for $\dot{e}_f(t)$ and $\dot{\eta}_m(t)$, respectively, and substituting (1-5) and (1-8) into (B–2) for $\ddot{x}_m(t)$, the expression for $\bar{M}\left(x_r\right) \ddot{x}_{rd}(t)$ in the linear parameterization in (3-17) can be determined without requiring acceleration measurements.

REFERENCES

[1] W. E. Dixon, M. S. de Queiroz, D. M. Dawson, and F. Zhang, "Tracking Control of Robot Manipulators with Bounded Torque Inputs," *Robotica,* Vol. 17, pp. 121-129, (1999).

[2] B. Brogliato, *Nonsmooth Impact Mechanics*, London, U.K.: Springer-Verlag, 1996.

[3] B. Brogliato, S. I. Niculescu, and P. Orhant, "On the Control of Finite-Dimentional Mechanical Systems with Unilateral Constraints," *IEEE Transactions on Automatic Control*, Vol. 42, No. 2, pp. 200-215, (1997).

[4] B. Brogliato and A. Zavala Rio, "On the Control of Complementary-Slackness Juggling Mechanical Systems," *IEEE Transactions on Automatic Control*, Vol. 45, No. 2, pp. 235-246, (2000).

[5] X. Cyril, G. J. Jarr, and A. K. Misra, "The Effect of Payload Impact on the Dynamics of a Space Robot," *Proceedings of the IEEE/RSJ International Conference on Intelligent Robots and Systems,* Yokohama, Japan, 1993, Vol. 3, pp. 2070-2075.

[6] M. Indri and A. Tornambe, "Control of Under-Actuated Mechanical Systems Subject to Smooth Impacts," *Proceedings of the IEEE Conference on Decision and Control*, Atlantis, Paradise Island, Bahamas, 2004, pp. 1228-1233.

[7] D. Materassi, M. Basso, and R. Genesio, "A Model for Impact Dynamics and its Application to Frequency Analysis of Tapping-Mode Atomic Force Microscopes," *Proceedings of the IEEE Conference on Decision and Control*, 2004, Vol. 6, pp. 6218-6223.

[8] L. Menini and A. Tornambe, "Asymptotic Tracking of Periodic Trajectories for a Simple Mechanical System Subject to Nonsmooth Impacts," *IEEE Transactions on Automatic Control*, Vol. 46, No. 7, pp. 1122-1126, (2001).

[9] P. Sekhavat, Q. Wu, and N. Sepehri, "Impact Control in Hydraulic Actuators with Friction: Theory and Experiments," *Proceedings of the American Control Conference,* Boston, Massachusetts, 2004, pp. 4432-4437.

[10] A. Tornambe, "Modeling and Control of Impact in Mechanical Systems: Theory and Experimental Results," *IEEE Transactions on Automatic Control*, Vol. 44, No. 2, pp. 294-309, (1999).

[11] R. Volpe and P. Khosla, "A Theoretical and Experimental Investigation of Impact Control for Manipulators," *International Journal of Robotics Research*, Vol. 12, No. 4, pp. 670-683, (1994).

[12] K. Yoshida, C. Mavroidis, and S. Dubowsky, "Impact Dynamic of Space Long Reach Manipulators," *Proceedings of the IEEE International Conference on Robotics and Automation,* Minneapolis, Minnesota, 1996, Vol. 3, pp. 1909-1916.

[13] K. Dupree, W. E. Dixon, G. Hu, and C. Liang, "Lyapunov-Based Control of a Robot and Mass-Spring System Undergoing An Impact Collision," *Proceedings of the IEEE American Control Conference,* Minneapolis, MN, 2006, pp. 3241-3246.

[14] K. Dupree, C. Liang, G. Hu, and W. E. Dixon, "Global Adaptive Lyapunov-Based Control of a Robot and Mass-Spring System Undergoing an Impact-Collision," *Proceedings of the IEEE Conference on Decision and Controls,* San Deigo, California, 2006, pp. 2039-2044.

[15] K. Dupree, C. Liang, G. Hu, and W. E. Dixon, "Global Adaptive Lyapunov-Based Control of a Robot and Mass-Spring System Undergoing an Impact Collision," *IEEE Transactions on Robotics,* submitted, 2006.

[16] G. Hu, W. E. Dixon, and C. Makkar, "Energy-Based Nonlinear Control of Under-Actuated Euler-Lagrange Systems Subject to Impacts," *Proceedings of the IEEE Conference on Decision and Control*, Seville, Spain, 2005, pp. 6859-6864.

[17] K. Youcef-Toumi and D. A. Guts, "Impact and Force Control," *Proceedings of the IEEE International Conference on Robotics and Automation,* Scottsdale, AZ, 1989, vol. 1, pp. 410-416.

[18] M. Indri and A. Tornambe, "Impact Model and Control of Two Multi-DOF Cooperating Manipulators," *IEEE Transactions on Automatic Control*, Vol. 44, No. 6, pp. 1297-1303, (1999).

[19] Ian D. Walker, "The Use of Kinematic Redundancy in Reducing Impact and Contact Effects in Manipulation," *Proceedings of the IEEE International Conference on Robotics and Automation,* Cincinnati, OH, 1990, vol. 1, pp. 434-439.

[20] Matthew Wayne Gertz, Jin-Oh Kim, and Pradeep K. Khosla, "Exploiting Redundancy to Reduce Impact Force," *IEEE/RSJ International Workshop on Intelligent Robots and Systems IROS,* Osaka, Japan, 1991, pp. 179-184.

[21] I. D. Walker, "Impact Configurations and Measures for Kinematically Redundant and Multiple Armed Robot Systems," *IEEE Transactions on Robotics and Automation,* Vol. 10, No. 5**,** pp 346-351, (1994).

[22] D. Chiu and S. Lee, "Robust Jump Impact Controller for Manipulators," *Proceedings of the IEEE/RSJ International Conference on Intelligent Robots and Systems*, Pittsburgh, Pennsylvania, 1995, Vol. 1, pp. 299-304.

[23] A. Tornambe, "Global Regulation of a Planar Robot Arm Striking a Surface," *IEEE Transactions on Automatic Control*, Vol. 41, No. 10, pp. 1517-1521, (1996).

[24] P. R. Pagilla and B. Yu, "A Stable Transition Controller for Constrained Robots," *IEEE/ASME Transactions on Mechatronics*, Vol. 6, No. 1, pp. 65-74, (2001).

[25] James M. Hyde and Mark R. Cutkosky, "Contact Transition Control: An Experimental Study," *IEEE Control System,* Vol. 14, No. 1, pp. 25-31, (1994).

[26] Prasad Akella, Vicente Parra-Vega, Suguru Armoto, and Kazuo Tanie, "Discontinuous Model-based Adaptive Control for Robots Executing Free and Constrained Tasks," *Proceedings of the IEEE International Conference on Robotics and Automation,* San Diego, CA, 1994, vol. 4, pp. 3000-3007.

[27] Tzyh-Jong Tarn, Yunying Wu, Ning Xi, and Alberto Isidori, "Force Regulation and Contact Transition Control," *IEEE Control System,* Vol. 16, Issue 1, pp. 32-40, (1996).

[28] Y. Wu, T. J. Tarn, N. Xi, and A. Isidori, "On Robust Impact Control via Positive Acceleration Feedback for Robot Manipulators," *Proceedings of the IEEE International Conference on Robotics and Automation*, Albuquerque, New Mexico, 1996, pp. 1891-1896.

[29] Eunjeong Lee, "Force and Impact Control for Robot Manipulators Using Time Delay," *IEEE International Symposium on Industrial Electronics,* 1999, pp. 151-156.

[30] E. Lee, et al., "Bang-Bang Impact Control Using Hybrid Impedance Time-Delay Control," *IEEE/ASME Transactions on Mechatronics*, Vol. 8, No. 2, pp. 272-277, (2003).

[31] Bradley J. Nelson, J. Daniel Morrow, and Pradeep K. Khosla, "Fast Stable Contact Transitions with a stiff Manipulator Using Force and Vision Feedback," *IEEE/RSJ International Conference on Intelligent Robots and Systems,* Pittsburgh, PA, 1995, Vol. 2, pp. 90-95.

[32] Yu Zhou, Bradley J. Nelson, and Barmeshwar Vikramaditya, "Fusing Force and Vision Feedback for Micromanipulation," *Proceedings of the IEEE International Conference on Robotics and Automation*, Leuven, Belgium, 1998, pp. 1220-1225.

[33] Ge Yang and Bradley J. Nelson, "Micromanipulation Contact Transition Control by Selective Focusing and Microforce Control," *Proceedings of the IEEE International Conference on Robotics and Automation*, Taipei, Taiwan, 2003, pp. 3200-3206.

[34] Masaaki Shibata and Takeshi Natori, "Impact Force Reduction for Biped Robot Based on Decoupling COG Control Scheme," *Proceedings of the IEEE International Workshop on Advanced Motion Control*, Nagoya, Japan, 2000, pp. 612-617.

[35] Eijiro Ohashi and Kouhei Ohnishi, "Motion Control in the Support Phase for a One-Legged Hopping Robot," *Proceedings of the IEEE International Workshop on Advanced Motion Control*, Kawasaki, Japan, 2004, pp. 259-262.

[36] Yoshiharu Sato, Eijiro Ohashi, and Kouhei Ohnishi, "Impact Force Reduction for Hopping Robot," *Conference of IEEE Industrial Electronics Society,* 2005, pp. 1821-1826.

[37] Rajiv V. Dubey, Tan Fung Chan, and Steve E. Everett, "Variable Damping Impedance Control of a Bilateral Telerobotic System," *IEEE Control Systems,* Vol. 17, Issue 1, pp. 37-45, (1997).

[38] Yoji Yamada, Yasuhiro Hirasawa, Shengyang Huang, Yoji Umetani, and Kazutsugu Suita, "Human-Robot Contact in the Safeguarding Space," *IEEE/ASME Transactions on Mechatronics,* Vol. 2, No. 4, pp. 230-236, (1997).

[39] Zhijun Li, Aiguo Ming, Ning Xi, Zhaoxian Xie, Jiangong Gu, and Makoto Shimojo, "Collision-Tolerant Control for Hybrid Joint based Arm of Non-holonomic Mobile Manipulator in Human-Robot Symbiotic Environments," *Proceedings of the IEEE International Conference on Robotics and Automation*, Barcelona, Spain, 2005, pp. 4037-4043.

[40] Panfeng Huang, Yangsheng Xu, and Bin Liang, "Contact and Impact Dynamics of Space Manipulator and Free-Flying Target," *IEEE/RSJ International Conference on Intelligent Robots and Systems,* 2005, pp. 1181-1186.

[41] W. E. Dixon, A. Behal, D. M. Dawson, and S. Nagarkatti, *Nonlinear Control of Engineering Systems: A Lyapunov-Based Approach*, Birkhäuser Boston, 2003.

[42] W. E. Dixon, E. Zergeroglu, D. M. Dawson, and M. W. Hannan, "Global Adaptive Partial State Feedback Tracking Control of Rigid-Link Flexible-Joint Robots," *Robotica*, Vol. 18. No 3. pp. 325-336, (2000).

[43] Z. Cai, M.S. de Queiroz, and D.M. Dawson, "A Sufficiently Smooth Projection Operator," *IEEE Transactions on Automatic Control*, Vol. 51, No. 1, pp. 135-139, (2006).

[44] M. Loffler, N. Costescu, and D. Dawson, "Qmotor 3.0 and the Qmotor Robotic Toolkit - An Advanced PC-Based Real-Time Control Platform," *IEEE Control Systems Magazine*, Vol. 22, No. 3, pp. 12-26, (2002).

[45] http://www.mae.ufl.edu/~dixon/projects/robman/impact.htm .

[46] http://www.mae.ufl.edu/~dixon/projects/robman/adaptiveimpact.htm .

BIOGRAPHICAL SKETCH

Chien-Hao Liang was born in Taipei, Taiwan. He completed his Bachelor in Ocean Enfineering in the year 2001 from National Taiwan University, Taipei. After finishing his military service, he joined the nonlinear controls and robotics research group in the University of Florida for Master of Science in mechanical and aerospace engineering in the year 2005.